UNIVERSITÀ DEGLI STUDI DI PADOVA

Facoltà di Scienze MM.NN.FF.

ISTITUTO NAZIONALE DI FISICA NUCLEARE

Laboratori Nazionali di Legnaro

in collaboration with Confindustria Veneto

MASTER THESIS

in

"Surface Treatments for Industrial Applications"

Title

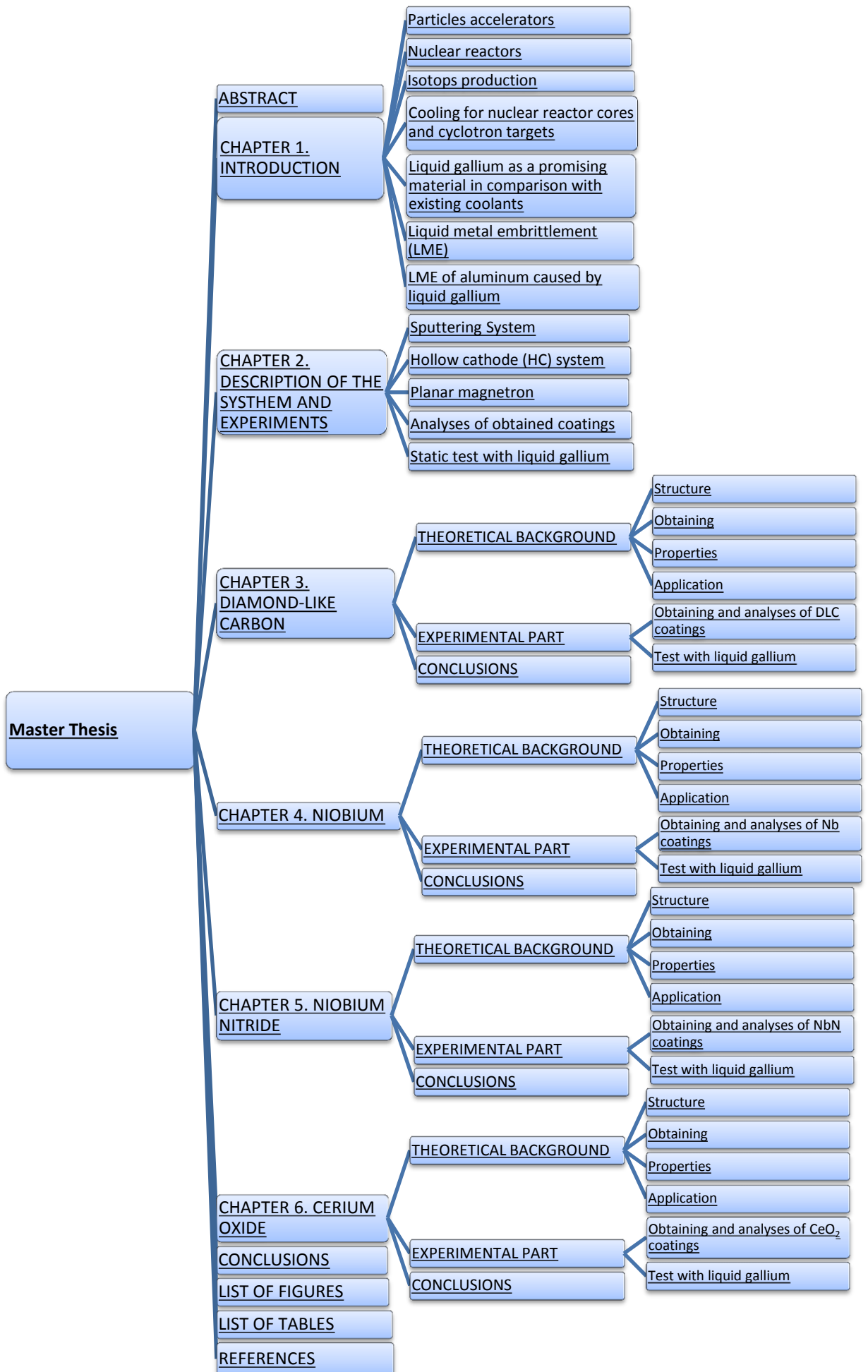# Protective Thin Films against Liquid Metal Embrittlement

Supervisor: Prof. V.Palmieri

Co-Supervisor:Dr. O.Azzolini

Candidate: Olga Cherenkova

Academic Year 2010-2011

Master Thesis

- ABSTRACT
- CHAPTER 1. INTRODUCTION
  - Particles accelerators
  - Nuclear reactors
  - Isotops production
  - Cooling for nuclear reactor cores and cyclotron targets
  - Liquid gallium as a promising material in comparison with existing coolants
  - Liquid metal embrittlement (LME)
  - LME of aluminum caused by liquid gallium
- CHAPTER 2. DESCRIPTION OF THE SYSTHEM AND EXPERIMENTS
  - Sputtering System
  - Hollow cathode (HC) system
  - Planar magnetron
  - Analyses of obtained coatings
  - Static test with liquid gallium
- CHAPTER 3. DIAMOND-LIKE CARBON
  - THEORETICAL BACKGROUND
    - Structure
    - Obtaining
    - Properties
    - Application
  - EXPERIMENTAL PART
    - Obtaining and analyses of DLC coatings
    - Test with liquid gallium
  - CONCLUSIONS
- CHAPTER 4. NIOBIUM
  - THEORETICAL BACKGROUND
    - Structure
    - Obtaining
    - Properties
    - Application
  - EXPERIMENTAL PART
    - Obtaining and analyses of Nb coatings
    - Test with liquid gallium
  - CONCLUSIONS
- CHAPTER 5. NIOBIUM NITRIDE
  - THEORETICAL BACKGROUND
    - Structure
    - Obtaining
    - Properties
    - Application
  - EXPERIMENTAL PART
    - Obtaining and analyses of NbN coatings
    - Test with liquid gallium
  - CONCLUSIONS
- CHAPTER 6. CERIUM OXIDE
  - THEORETICAL BACKGROUND
    - Structure
    - Obtaining
    - Properties
    - Application
  - EXPERIMENTAL PART
    - Obtaining and analyses of CeO_2 coatings
    - Test with liquid gallium
  - CONCLUSIONS
- CONCLUSIONS
- LIST OF FIGURES
- LIST OF TABLES
- REFERENCES

CONTENTS

ABSTRACT

A nuclear reactor is a system that contains and controls sustained nuclear chain reactions. Reactors are used for generating electricity, moving aircraft carriers and submarines, producing medical isotopes for imaging and cancer treatment, and for conducting research. Fuel, made up of heavy atoms that split when they absorb neutrons, is placed into the reactor vessel (basically a large tank) along with a small neutron source. The neutrons start a chain reaction where each atom that splits releases more neutrons that cause other atoms to split. Each time an atom splits, it releases large amounts of energy in the form of heat. The heat is carried out of the reactor by coolant, which is most commonly just plain water. The coolant heats up and goes off to a turbine to spin a generator or drive shaft. So basically, nuclear reactors are exotic heat sources.

Cyclotrons continue to be efficient accelerators for radio-isotope production. In recent years, developments in the accelerator technology have greatly increased the practical beam current in these machines while also improving the overall system reliability. These developments combined with the development of new isotopes for medicine and industry, and a retiring of older machines indicates a strong future for commercial cyclotrons.

For both systems, efficient cooling is required. Nowadays liquid metals are in wide use for this purpose. Liquid metal cooled reactors were first adapted for nuclear submarine use but have also been extensively studied for power generation applications. Liquid metals have safety advantages because they have high heat transfer characteristics, due to high boiling point, no high vapor pressure, and they allow a much higher power density than traditional coolants. Cooling by liquid mercury, sodium, NaK, lead has been studied and used. But due to numerous imperfections of these coolants (such as toxicity, high vapor pressure, not appropriate melting/boiling points, corrosion etc) it is necessary to develop new cooling systems for research and industrial purposes.

Thus after choosing the new coolants (liquid metals with desirable properties) for target cooling we will develop the protection coatings for tubes taking into account factors which influence corrosion such as solution pH, oxidizing agent, temperature, velocity, stresses, impurity content.

So we can conclude that development of new protective thin films, coatings, claddings are required and mandatory for protection. For its development we propose to use the magnetron sputtering which is a very perspective method for obtaining of thin films. One feature of magnetron sputtering which explains its wide use for the coatings is the low charged particle fluxes reaching a substrate. By this method we can obtain coatings on conductive materials as well

as on nonconductive, also on materials with low melting points. Sputtered films typically have a better adhesion on the substrate than evaporated films.

Thereby the producing of protective coatings from liquid metals coolants embrittlement used for nuclear reactors and target cooling in the radiopharmaceutical sphere has been under development within the bounds of this project.

CHAPTER 1. INTRODUCTION

In this chapter the short overview of some systems, which require efficient liquid metal cooling and hence protection of these cooling systems from LME, is given.

1.1 Particles accelerators

A *cyclotron* is a type of particle accelerator. Cyclotrons accelerate charged particles using a high-frequency, alternating voltage (potential difference). A perpendicular magnetic field causes the particles to spiral almost in a circle so that they re-encounter the alternating voltage many times (Fig.1.1).
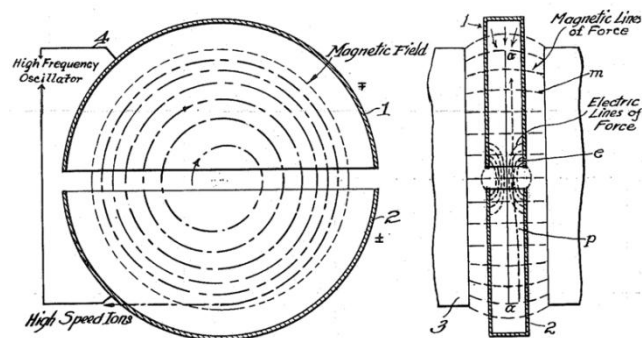
Fig.1. 1 Diagram of cyclotron operation from Lawrence's 1934 patent

The electrodes shown at the right would be in the vacuum chamber, which is flat, in a narrow gap between the two poles of a large magnet. In the cyclotron, a high-frequency alternating voltage applied across the "D" electrodes (also called "Dees") alternately attracts and repels charged particles. The particles, injected near the center of the magnetic field, increase in speed (and therefore energy) only when passing through the gap between the electrodes. The perpendicular magnetic field (passing vertically through the "D" electrodes), combined with the increasing energy of the particles forces the particles to travel in a spiral path. With no change in energy the charged particles in a magnetic field will follow a circular path. In the cyclotron, energy is applied to the particles as they cross the gap between the "Dees" and so they are accelerated (at the typical sub-relativistic speeds used) and will increase in mass as they approach the speed of light. Either of these effects (increased velocity or increased mass) will increase the radius of the circle and so the path will be a spiral. (The particles move in a spiral, because a current of electrons or ions, flowing perpendicular to a magnetic field, experiences a force perpendicular to its direction of motion. The charged particles move freely in a vacuum, so the particles follow a spiral path). The radius will increase until the particles hit a target at the perimeter of the vacuum chamber. Various materials may be used for the target, and the collisions will create secondary particles which may be guided outside of the cyclotron and into instruments for analysis. The

results will enable the calculation of various properties, such as the mean spacing between atoms and the creation of various collision products. Subsequent chemical and particle analysis of the target material may give insight into nuclear transmutation of the elements used in the target.

For several decades, cyclotrons were the best source of high-energy beams for nuclear physics experiments; several cyclotrons are still in use for this type of research. Cyclotrons can be also used to treat cancer. Ion beams from cyclotrons can be used, as in proton therapy, to penetrate the body and kill tumors by radiation damage, while minimizing damage to healthy tissue along their path. Cyclotron beams can be used to bombard other atoms to produce short-lived positron-emitting isotopes suitable for PET imaging.

The cyclotron was an improvement over the *linear accelerators* (Fig.1.2) that were available when it was invented. A linear accelerator (also called a linac) accelerates particles in a straight line through an evacuated tube (or series of such tubes placed end to end). A set of electrodes shaped like flat donuts are arranged inside the length of the tube(s). These are driven by high-power radio waves that continuously switch between positive and negative voltage, causing particles traveling along the center of the tube to accelerate. In the 1920s, it was not possible to get high frequency radio waves at high power, so either the accelerating electrodes had to be far apart to accommodate the low frequency or more stages were required to compensate for the low power at each stage. Either way, higher-energy particles required longer accelerators than scientists could afford.

Fig.1. 2 Linear particle accelerator in California

Modern linacs use high power Klystrons and other devices able to impart much more power at higher frequencies. But before these devices existed, cyclotrons were cheaper than linacs. Cyclotrons accelerate particles in a spiral path. Therefore, a compact accelerator can contain much more distance than a linear accelerator, with more opportunities to accelerate the particles.

The spiral path of the cyclotron beam can only "sync up" with klystron-type (constant frequency) voltage sources if the accelerated particles are approximately obeying Newton's Laws of Motion. If the particles become fast enough that relativistic effects become important, the beam gets out of phase with the oscillating electric field, and cannot receive any additional acceleration. The cyclotron is therefore only capable of accelerating particles up to a few percent of the speed of light. To accommodate increased mass the magnetic field may be modified by appropriately shaping the pole pieces as in the isochronous cyclotrons, operating in a pulsed mode and changing the frequency applied to the "Dees" as in the synchrocyclotrons, either of which is limited by the diminishing cost effectiveness of making larger machines. Cost limitations have been overcome by employing the more complex synchrotron or linear accelerator, both of which have the advantage of scalability, offering more power within an improved cost structure as the machines are made larger.

1.2 Nuclear reactors

A nuclear reactor is a device to initiate and control a sustained nuclear chain reaction. Most commonly they are used for generating electricity and for the propulsion of ships. Usually heat from nuclear fission is passed to a working fluid (water or gas), which runs through turbines that power either ship's propellers or generators. Some produce isotopes for medical and industrial use, and some are run only for research (Fig.1.3).
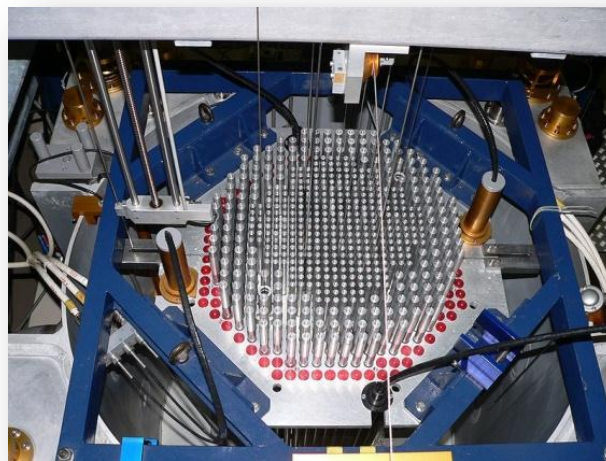
Fig.1. 3 Core of CROCUS, a small nuclear reactor used for research at the EPFL in Switzerland

Just as conventional power stations generate electricity by harnessing the thermal energy released from burning fossil fuels, nuclear reactors convert the thermal energy released from nuclear fission. This nuclear chain reaction can be controlled by using neutron poisons and

neutron moderators to change the portion of neutrons that will go on to cause more fissions[1]. Nuclear reactors generally have automatic and manual systems to shut the fission reaction down if unsafe conditions are detected[2].

The reactor core generates heat in a number of ways:

- The kinetic energy of fission products is converted to thermal energy when these nuclei collide with nearby atoms.

- Some of the gamma rays produced during fission are absorbed by the reactor, their energy being converted to heat.

- Heat produced by the radioactive decay of fission products and materials that have been activated by neutron absorption. This decay heat source will remain for some time even after the reactor is shut down.

1.3 Isotops production

Nuclear technology is currently used in nearly every field and aspect of our lives from medicine, to manufacturing and construction, to powering common household items, and to producing electricity for over 16% of worldwide needs.

The use of radionuclides in the physical and biological sciences can be broken down into three general categories; imaging, radiotherapy and radiotracers. Imaging can be further divided into PET and SPECT.

In internal radiotherapy for treating cancer and other diseases, the second principle is, in a strict sense, broken since the purpose of delivering the radiotoxic substance is to have the emitted radiation cause damage to the tumour tissues. However, in order for the radiotoxic substance to be localized, it must follow the known chemical behaviour without perturbing that pathway.

Most of the radiotracers used in vivo should have relatively short half-lives (less than a few hours to at most a few days). There are definite advantages in using short lived radionuclides; for example, there is a low radiation dose associated with each study, serial studies are possible (sometimes on the same day for tracers such as 11C) and radioactive waste disposal problems are minimized if not eliminated. The disadvantages are the need for an accelerator nearby or within easy shipping distance for the longer lived species (a few hours), and for rapid chemical procedures, especially for formation of more complex compounds.

Radionuclide production is converting the atoms of one element into those of another. This conversion involves altering the number of protons and/or neutrons in the nucleus (target). If a neutron is added without the emission of particles, then the resulting nuclide will have the same

chemical properties as those of the target nuclide. If, however, the target nucleus is bombarded by a charged particle, for example a proton, the resulting nucleus will usually be that of a different element. The exact type of nuclear reactions a target undergoes depends on a number of parameters, including the type and energy of the bombarding particle.

The production of radionuclides with an accelerator demands that particle beams be delivered with two specific characteristics. The beam must have sufficient energy to bring about the required nuclear reactions, and there must be sufficient beam current to give practical yields.

There are literally hundreds of radioisotopes that can be produced with charged particle accelerators. The cyclotron is the most frequent choice of accelerator, but the linac and other accelerators may become more common with the development of smaller, more reliable, machines.

The goal of cyclotron targetry is to place the target material into the beam, keep it there during irradiation, and remove the product radionuclide from the target material quickly and efficiently. The specific design of the target is what allows this goal to be achieved. Unless care is taken in the design and fabrication of the target, the production of the radioisotope can be far from optimal and may even be impossible. Over time, many facilities will need to increase the number of radioisotopes being produced or to optimize the yields of their currently produced radioisotopes. If an increase in production with commercial targets is being sought, modifications of existing targets and procedures or development of new targets may be ways of accomplishing this objective.

1.4 Cooling for nuclear reactor cores and cyclotron targets

As was mentioned earlier, the energy lost when charged particles pass through the target medium is dissipated in the form of heat. One of the most challenging problems in the design of cyclotron targets is finding methods to remove this heat from the target during irradiation. The heat generated in the target often has several detrimental effects. A few of these, such as reduction of target density, chemical reactions occurring in the target material or products, as well as possible damage to the target foil or body, occur.

A nuclear reactor coolant is being needed to remove the heat from the nuclear reactor core and transfer it to electrical generators and the environment. Frequently, a chain of two coolant loops are used because the primary coolant loop takes on short-term radioactivity from the reactor.

Nowadays, coolants, such as water, molten salts and metals, gases are being in use.

Almost all currently operating nuclear power plants are light water reactors using ordinary water under high pressure as coolant and neutron moderator. About 1/3 are boiling water reactors where the primary coolant undergoes phase change to steam inside the reactor. About 2/3 are pressurized water reactors at even higher pressure. Current reactors stay under the critical point at around 374 °C and 218 bar where the distinction between liquid and gas disappears, which limits thermal efficiency, but the proposed supercritical water reactor would operate above this point.

Heavy water reactors use deuterium oxide which has similar properties to ordinary water but much lower neutron capture, allowing more thorough moderation.

Fast reactors have a high power density and do not need neutron moderation. Most have been liquid metal cooled reactors using molten sodium. Lead, lead-bismuth eutectic, and other metals have also been proposed and occasionally used. Mercury was used in the first fast reactor.

Molten salts share with metals the advantage of low vapor pressure even at high temperatures, and are less chemically reactive than sodium. Salts containing light elements like fluor, lithium, berillium can also provide moderation. In the Molten-Salt Reactor Experiment it even served as a solvent carrying the nuclear fuel.

Gases have also been used as coolant. Helium is extremely inert both chemically and with respect to nuclear reactions but has a low heat capacity, necessitating rapid circulation. Carbon dioxide has also been used in advanced gas-cooled reactor. Gases of course need to be under pressure for sufficient density at high temperature[3].

1.5 Liquid gallium as a promising material in comparison with existing coolants

Liquid metal coolants are used in a fast reactors and cyclotrons for isotops production, have included sodium, such as NaK, lead, lead-bismuth eutectic, and in early reactors, mercury. This is a reactor design that is cooled by liquid metal, totally unmoderated, and produces more fuel than it consumes. They are said to "breed" fuel, because they produce fissionable fuel during operation because of neutron capture. These reactors can function much like a pressurized water reactors in terms of efficiency, and do not require much high pressure containment, as the liquid metal does not need to be kept at high pressure, even at very high temperatures. BN-350 and BN-600 in USSR and Superphénix in France were a reactor of this type, as was Fermi-I in the United States. The Monju reactor in Japan suffered a sodium leak in 1995 and was restarted in May 2010. All of them use/used liquid sodium. These reactors are fast neutron, not thermal neutron designs.

Using lead as the liquid metal provides excellent radiation shielding, and allows for operation at very high temperatures. Also, lead is (mostly) transparent to neutrons, so fewer neutrons are lost in the coolant, and the coolant does not become radioactive. Unlike sodium, lead is mostly inert, so there is less risk of explosion or accident, but such large quantities of lead may be problematic from toxicology and disposal points of view. Often a reactor of this type would use a lead-bismuth eutectic mixture. In this case, the bismuth would present some minor radiation problems, as it is not quite as transparent to neutrons, and can be transmuted to a radioactive isotope more readily than lead. The Russian Alfa class submarine uses a lead-bismuth-cooled fast reactor as its main power plant.

Most Liquid Metal Cooled Fast Breeder Reactors are of this type. The sodium is relatively easy to obtain and work with, and it also manages to actually prevent corrosion on the various reactor parts immersed in it. However, sodium explodes violently when exposed to water, so care must be taken, but such explosions would not be vastly more violent than (for example) a leak of superheated fluid from a Supercritical Water Reactor or Pressurized Water Reactors. Experimental Breeder reactor (EBR-I), the first reactor to have a core meltdown, was of this type.

To compare to other metal coolants (*Table 1.1*)*, liquid gallium* is a promising perspective for this purpose. This study suggests gallium as potential coolant for the next generation reactor because of its low melting point (29°C), high boiling point (2204°C), and high safety against explosion. However, gallium is relatively high thermal neutron absorption material. To reduce absorption cross-section, ternary was considered as Ga-Sn-Zn. Tin and zinc have lower cross-section than gallium, and alloying with gallium can have another advantage that it has lower melting point[4].

*Table 1. 1 Melting and boiling points for some existing coolants*

Coolant	Melting point, ˚C	Boiling point, ˚C
Water	0	100
Sodium	97	883
NaK	-11	785
Mercury	-38	357
Lead	327	1749
Lead-bismuth eutectic	123	1670
Gallium	29	2204

Also, gallium has a high affinity for many metals and alloys, especially steels. The most competitive materials interacted with gallium were refractory metals such as tungsten. Gallium penetrates between grain boundaries of a metal and causes the embrittlement.

A lot of compounds, mainly oxides, as protective coatings have been studied to prevent corrosion by forming a protective layer on structural material alloys. This barrier on the surface can help to prevent corrosion occurring at the interface.

1.6 Liquid metal embrittlement (LME)

Liquid metal embrittlement (also known as liquid metal induced embrittlement) is a phenomenon of practical importance, where certain ductile metals experience drastic loss in tensile ductility or undergo brittle fracture when tested in the presence of specific liquid metals (Fig. 1.4).
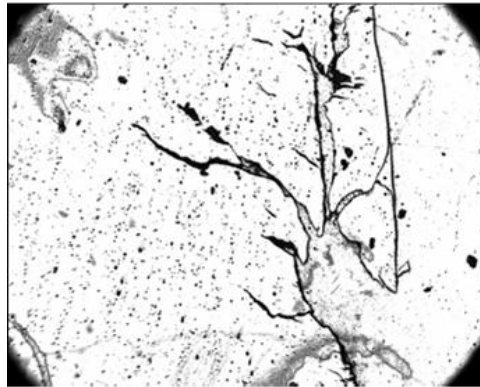
Fig.1. 4 LME caused by liquid aluminum penetrating into cobalt-nikel alloy

Generally, a tensile stress, either externally applied or internally present, is needed to induce embrittlement. Exceptions to this rule have been observed, as in the case of aluminium and other metals in the presence of liquid gallium[5]. People have studied this phenomenon from the beginning of the 20th century. Many of its phenomenological characteristics are known and several mechanisms were proposed to explain it[6,7]. The practical significance of liquid metal embrittlement is revealed by the observation that several steels experienced ductility losses and cracking during hot dip galvanizing or during subsequent fabrication[8]. Cracking can occur catastrophically and very high crack growth rates have been measured.

Liquid metal embrittlement or LME is characterized by the reduction in the threshold stress intensity, true fracture stress or in the strain to fracture when tested in the presence of liquid metals as compared to that obtained in air/vacuum tests. The reduction in fracture strain is generally temperature dependent and a "ductility drop" is observed as the test temperature is

decreased[9]. A ductile-to-brittle transition behaviour is also exhibited by many metal couples. The shape of the elastic region of the stress-strain curve is not altered, but the plastic region may be changed during LME. Very high crack propagation rates, varying from few centimeters per second to several meters per second are induced in solid metals by the embrittling liquid metals. An incubation period and a slow pre-critical crack propagation stage generally precede final fracture.

It is believed that there is specificity in the solid-liquid metals combinations experiencing LME[10]. There should be limited mutual solubilities for the metal couple to cause embrittlement. Excess solubility makes sharp crack propagation difficult, but no solubility condition prevents wetting of the solid surfaces by liquid metal and prevents LME. Presence of an oxide layer on the solid metal surface also prevents good contact between the two metals and stops LME. The chemical compositions of the solid and liquid metals affect the severity of embrittlement. Addition of third elements to the liquid metal may increase or decrease the embrittlement and alters the temperature region over which embrittlement is seen. Metal combinations which form intermetallic compounds do not cause LME. There are a wide variety of LME couples[11]. Most technologically important are the LME of aluminum and steel alloys.

Grain size greatly influences LME. Solids with larger grains are more severely embrittled and the fracture stress varies inversely with the square root of grain diameter. Also the brittle to ductile transition temperature is increased by increasing grain size.

External parameters like temperature, strain rate, stress and time of exposure to the liquid metal prior to testing affect LME. Temperature produces a ductility trough and a ductile to brittle transition behaviour in the solid metal. The temperature range of the trough as well as the transition temperature are altered by the composition of the liquid and solid metals, the structure of the solid metal and other experimental parameters. The lower limit of the ductility trough generally coincides with the melting point of the liquid metal. The upper limit is strain rate sensitive. Temperature also affects the kinetics of LME. An increase in strain rate increases the upper limit temperature as well as the crack propagation rate. In most metal couples LME does not occur below a threshold stress level.

Many theories have been proposed for LME. The major ones are listed below:

- The dissolution-diffusion model of Robertson[12] and Glickman[13] says that adsorption of the liquid metal on the solid metal induces dissolution and inward diffusion. Under stress these processes lead to crack nucleation and propagation.

- The brittle fracture theory of Stoloff and Johnson[14], Westwood and Kamdar[15] proposed that the adsorption of the liquid metal atoms at the crack tip weakens inter-atomic bonds and propagates the crack.
- Gordon[16] postulated a model based on diffusion-penetration of liquid metal atoms to nucleate cracks which under stress grow to cause failure.
- The ductile failure model of Lynch[17] and Popovich[18] predicted that adsorption of the liquid metal leads to weakening of atomic bonds and nucleation of dislocations which move under stress, pile-up and work harden the solid. Also dissolution helps in the nucleation of voids which grow under stress and cause ductile failure.

All of these models utilize the concept of an adsorption-induced surface energy lowering of the solid metal as the central cause of LME. They succeeded in predicting many of the phenomenological observations. However, a quantitative prediction of LME is still elusive.

1.7 LME of aluminum caused by liquid gallium

Polycrystalline aluminum becomes brittle if it is stressed after interaction with liquid gallium. This is a typical example of liquid metal embrittlement, which refers to the loss of ductility of normally ductile metals when stressed whilst in contact with a liquid metal. In the case of aluminum and gallium, it is also known that fracture stress and fracture strain are reduced above the melting point of gallium (29,8°C), even if it is stressed after gallium is removed from the surface of aluminum specimens. The fracture stress reduces with an increase in the contact time. This phenomenon is attributed to the penetration of gallium into the polycrystalline aluminum, which reduces the strength of grain boundaries[19].
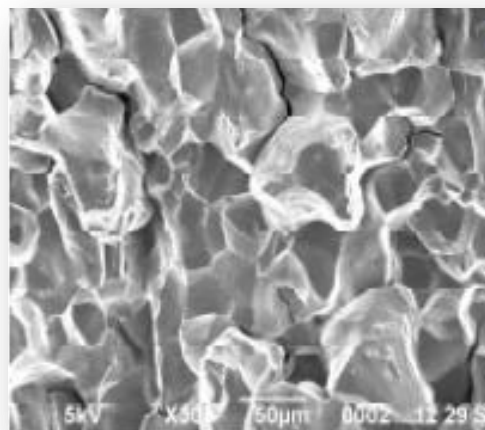
Fig.1. 5 SEM image of Al fracture caused by liquid Ga

The rapid penetration of gallium atoms has been confirmed by radiotracer[20], transmission electron microscope[21,22] and X-ray techniques[23,24].

SEM micrographs show that most of the fracture surface consists of smooth grain surfaces when the maximum stress is small, while the fracture surface is a mixture of intergranular and transgranular fracture surfaces when the maximum stress in large. This suggests that in this temperature range the number of weakened grain boundaries increases with temperature, even when gallium in the grain boundaries may not be in the liquid state. The penetration of gallium depends on the nature of grain boundaries of aluminum[25]; therefore, it can be expected that each grain boundary becomes weak at a different temperature.

CHAPTER 2. DESCRIPTION OF THE SYSTHEM AND EXPERIMENTS

2.1 Sputtering System

The sputtering system consists of 4 vacuum chambers connected through the central zone (Fig.2.1) and separated by Varian pneumatic gates CF63 in order to be able to carry on processes in different chambers in series.
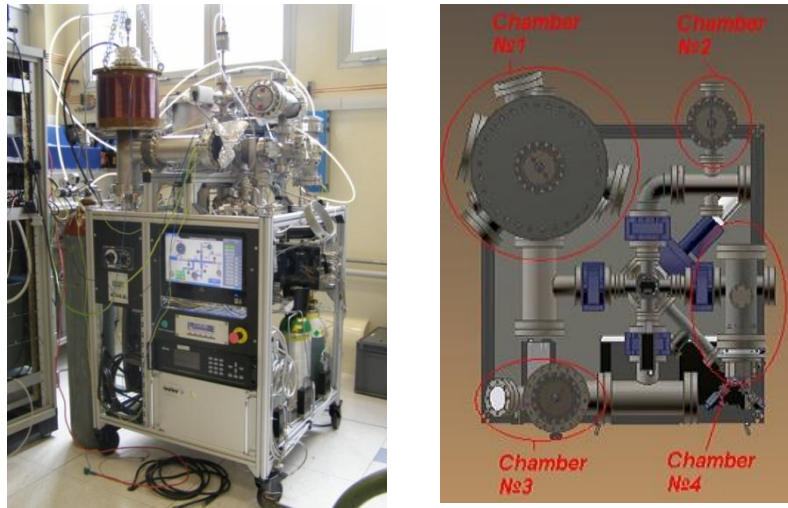
Fig.2. 1 Sputtering System

The Pfeiffer turbo molecular pump of 360 l/min and Varian Dry Scroll Pump 210 l/min as a primary pump provided base vacuum pressure up to 10E-6 mbar without backing. Full range gauge MaxiGauge™ TPG 256A measured pressure till 10E-10 mbar and was used while pumping. But for the process, at 10E-4 mbar, not sensitive to plasma, capacitance vacuummeter MKS was used (Fig.2.2).

Fig.2. 2 Full Range (a) and capacitance (b) gauges and corresponding control panels

The gases for sputtering – nitrogen, oxygen and argon (99,99% purity) were delivered through stainless steel pipes from gas cylinders to the central zone of the system. The gas flow

was controlled by mass flow meter MKS (Fig.2.2). In case of obtaining DLC coatings, gas acetylene was delivered from an external gas cylinder, the inlet was connected directly to the working chamber (№3) and the flow was controlled by a leak valve.

A Labview program was used to control pneumatic gates, pumping and venting of the sputtering system (Fig.2.3).
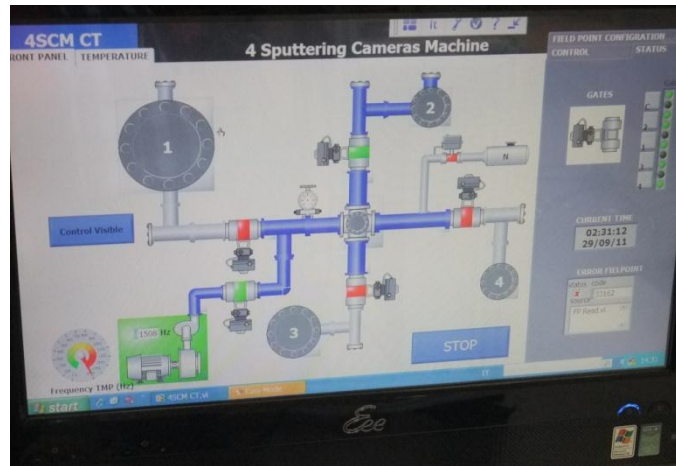
Fig.2. 3 Touch screen PC panel of LabView program for sputtering system control

2.2 Hollow cathode (HC) system

A magnetron sputtering source can be defined as a diode device in which magnetic fields are confined near the cathode surface to form electron traps which are so configured that the **E x B** electron-drift currents can close on cathode[26]. Cylindrical sputtering sources with post[27,28] or hollow cathodes[29], coaxial anodes, and axial magnetic fields have been reported for number of years (Fig.2.4)[30]. Remarkable performance is achieved when plasma is confined near the target by proper shaping of the magnetic field and by using suitably placed electron reflecting surfaces. High currents and sputtering yields can be obtained, at moderate and near constant voltages, even at low pressures. This characterizes what has been defined as the *magnetron mode of operation*[25]. It can also be obtained for plasma rings magnetically confined over planar surfaces (planar magnetrons)[31] or over short cylinders or within cylindrical surface cavities (sputter guns)[32].

A hollow cathode with uniform cosine emission has the interesting characteristic that the coating flux at all points within the cathode that are unaffected by end losses in equal to the cathode erosion flux, independent of the working gas pressure. This behavior has been experimentally verified. It makes hollow cathodes particularly effective for coating objects of complex shape. The charged particle densities on the axis are typically 1/3 that adjacent to the

target surface. Floating potentials are -20 to -50 V relative to anode. For metals the ion diffusion flux to the substrate is typically 1/5-1/3 the sputtered atom flux[33].
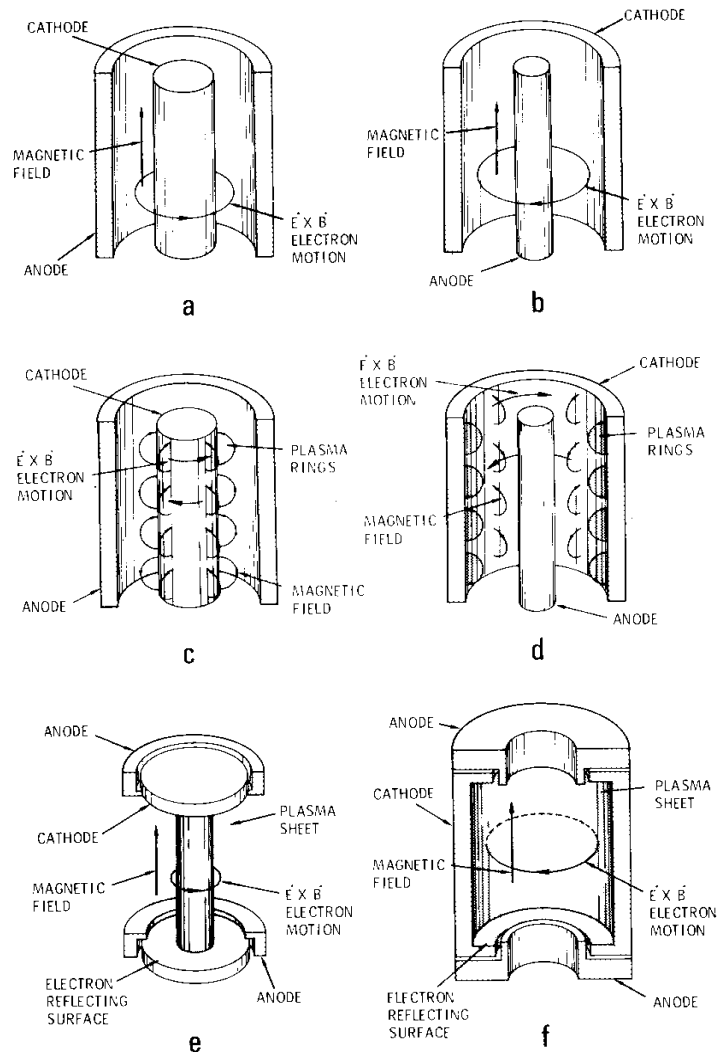

Fig.2. 4 The configuration of various cylindrical magnetron sputtering sources: a,b – general magnetron configurations, b,d,f – hollow cathodes (inverted magnetrons), e – cylindrical-post magnetron[33]

In this project for deposition of DLC (diamond like carbon) the hollow cathode was used (Fig.2.4 f). The experiments were carried out in a cylindrical, stainless steel vacuum chamber 11 cm in diameter and about 49 cm in length. The carbon cathode had a cylindrical hollow shape 10 mm thick with distance to the chamber wall 1 mm (Fig.2.5). On the top the system was equipped with water cooling system and inlet for acetylene gas.
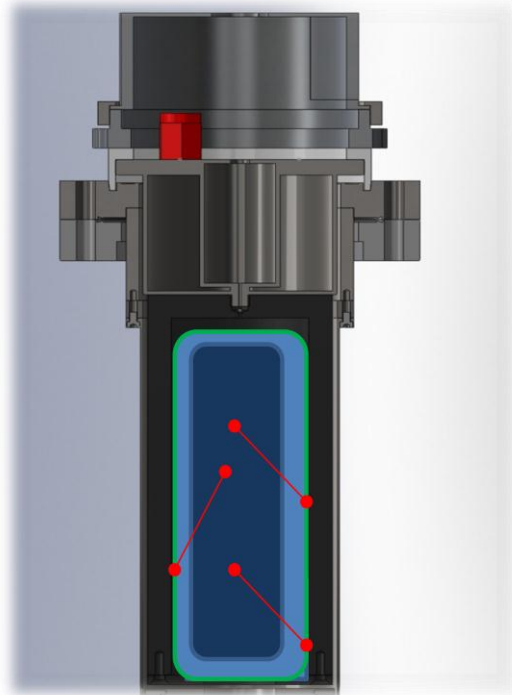
Fig.2. 5 Hollow carbon cathode for sputtering

The sample holder (Fig.2.6) with spirally assembled quartz samples was placed vertically in the hollow cathode chamber (Fig.2.1, №4). The design allowed applying of a voltage to the sample holder, so we could perform bias (negative potential) and substrate cleaning by plasma.
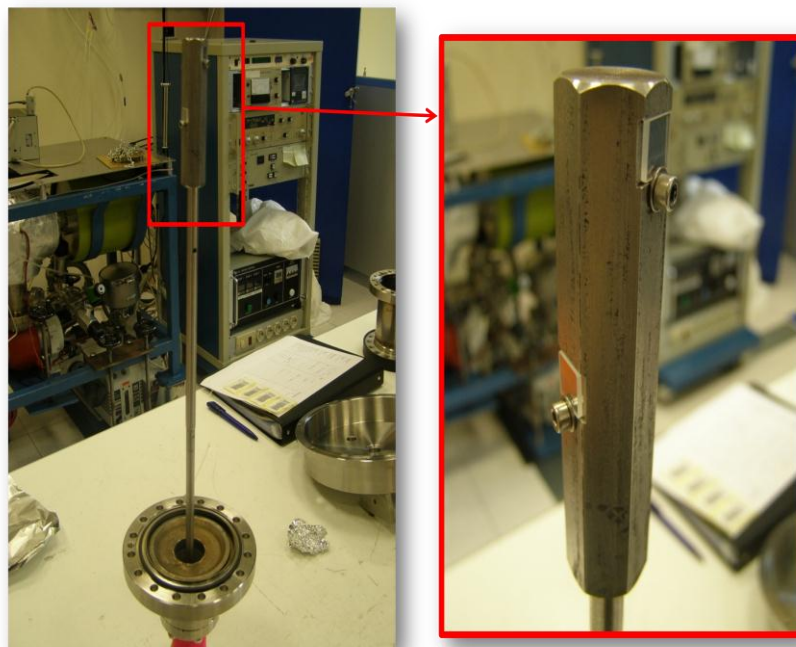
Fig.2. 6 Vertical sample holder

Before deposition, quartz substrates were cleaned in a following way: firstly in untrasonic bath for 30 min at 40 ˚C in Rodaclean solution (GNL), then in deionized water during 20 min, after

that samples were rinsed with ethanol and rests of alcohol were blew out by nitrogen gas flux until dry.

In order to confine electrons close to the hollow cathode surface, the external magnetic field (copper coil) was applied (Fig. 2.7).
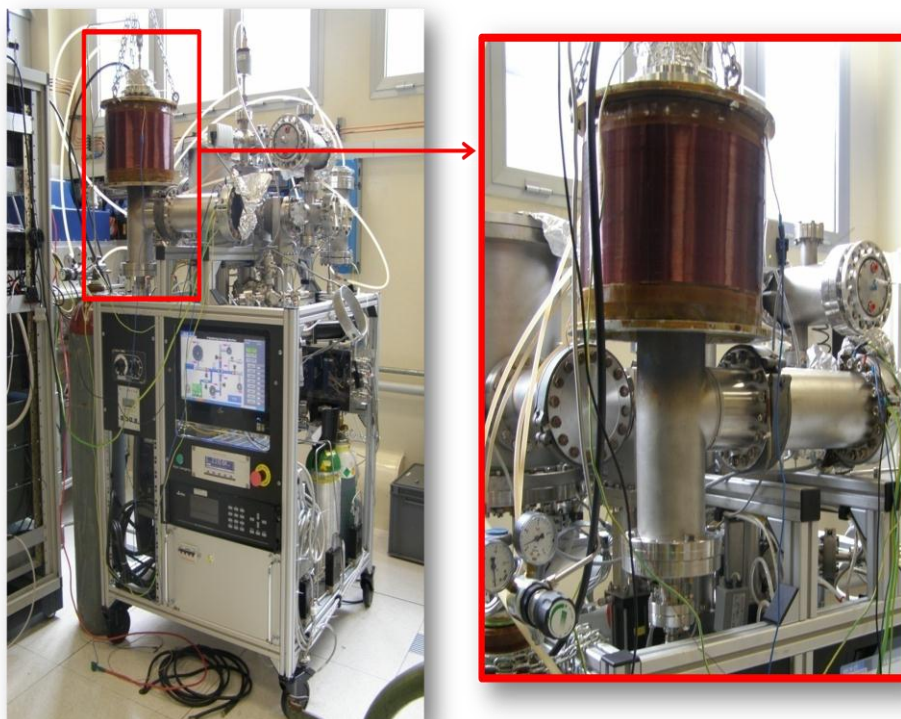
Fig.2. 7 Sputtering system

2.3 Planar magnetron

Planar sputtering magnetrons (Fig. 2.8) are important tools for thin film deposition and ion etching[34]. With some modification, planar magnetrons also have potential to become high intensity hyperthermal atomic beam sources[35].
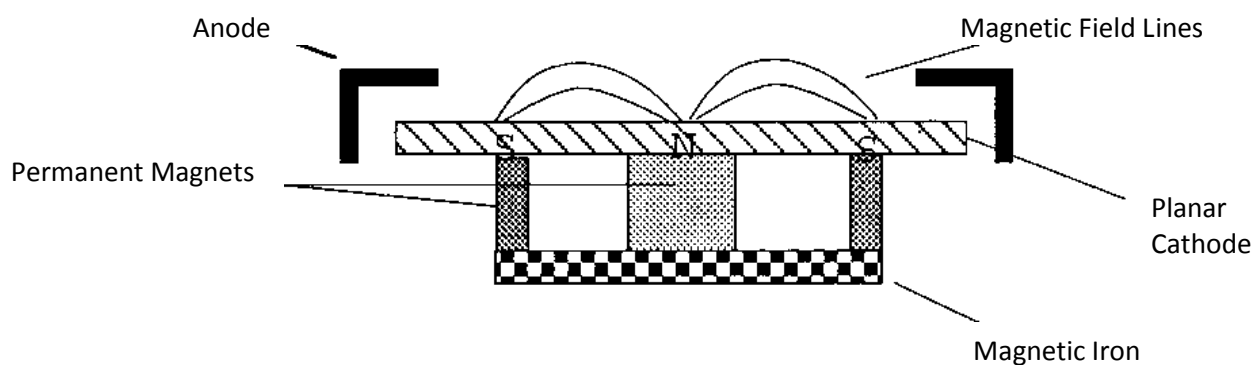
Fig.2. 8 Scheme of planar magnetron configuration

In *balanced* magnetrons, the discharge is confined by the magnetic field close to the cathode surface, and consequently the bombardment of the growing film by energetic particles (other than the depositing atoms) is minimal. However, there are many situations where the properties of the thin film are improved by bombarding the growing film with energetic ions[36],[37]. In *unbalanced* magnetrons plasma is dense also near substrate. Effects of ion bombardment during deposition include making the film more dense and preferentially orienting the crystallites in the deposit. The available technology for ion assisted deposition, particularly where separate sources are used for the deposition flux and the ion flux, is difficult to implement in many production situations.

For deposition of Nb, NbN and CeO$_2$ the *balanced planar magnetron* system was used. The experiments were carried out in a cylindrical, stainless steel vacuum chamber of 11 cm in diameter and 26 cm in length (Fig.2.9). The dimensions of the planar magnetron cathode (Nb, Ce targets), were 2 inches in diameter, and about 5 mm in thickness. The magnets must be cooled down during deposition because for NdFeB magnets, which we used in this project, even mild overheating will cause some permanent loss of magnetic field strength (Fig.2.9).
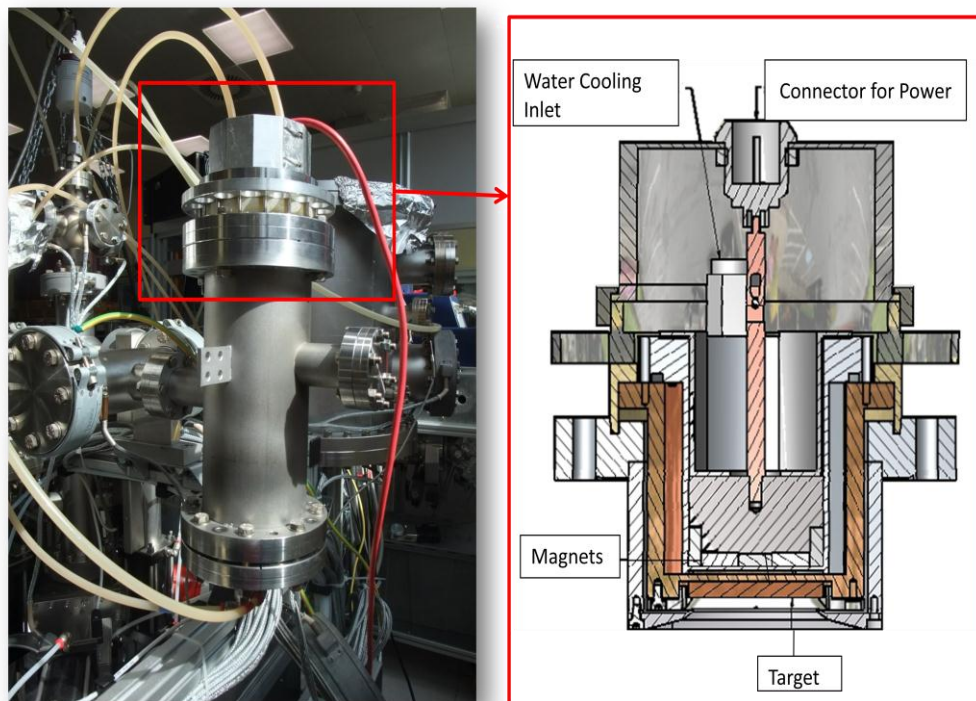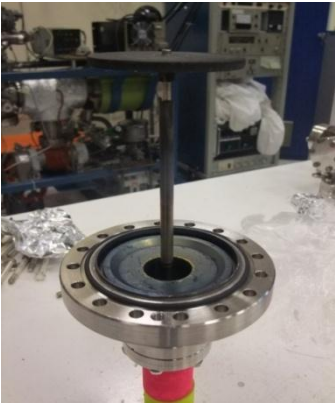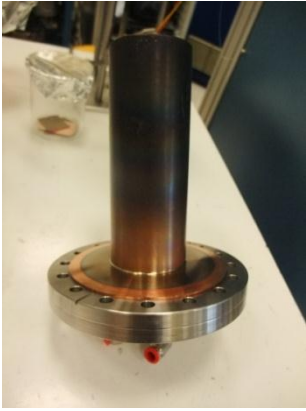
Fig.2. 9 Working chamber and planar magnetron for sputtering

The deposition was carried out on different planar sample holders with possibility to water cool or to heat up the substrate, to apply bias and to implement plasma cleaning of the substrate (Table.2.1).

Table 2. 1 Sample holders used in magnetron sputtering to obtain Nb, NbN and CeO₂ coatings

Sample Holder:		
Biased	Water Cooled	With Heating Element (IR)
Target-Substrate Distance:		
7,5 cm	6,5 cm	12,0 cm

As a substrate, aluminum foil (0,05 mm in thickness, the size varied for different sample holders) and quartz (5x5x1 mm) were used. Aluminum substrate was cleaned in a similar way as quartz (chapter 2.2), but as a soap, GP 17.40 SUP (NGL) was used. We must perform cleaning in a cold water and watch that aluminum does not stay in deionized water, which is a very aggressive environment, over 10 minues.

Aluminum was picked as a substrate because of its easiest solubility in liquid gallium. We believe that if we can protect aluminum from liquid Ga by coating, then these coatings would work as barriers for several other metals and alloys. And if not, the work of optimization of coating morphology and microstructure will be certainly useful for other systems.

2.4 Analyses of obtained coatings

In order to measure the film thickness, a part of the substrate was masked during the deposition. A Contact Profilometer Dektak 8 was used for the measurement of the height of the step from the bare substrate to the top of the deposited film. The diamond stylus had 2,5 μm diameter and its force, used in this work, was 10 mg in the measurement range of 65500 nm and for hills and valleys profile. Thereby, we obtained thickness and surface maps of our coatings.

By Thin Film Diffraction method, grown on bulk substrate coatings were characterized. For this purpose we used Philips Xpert Diffractometer with a copper X-Ray tube. Using X-Pert computer software the XRD patterns were fitted in order to obtain the peak position, integral breadth and the integrated peak surface (peak intensity).

From obtained data we calculated cubic lattice parameters:

$$a = \sqrt{(h^2 + k^2 + l^2).d_{hkl}^2},\text{ where}$$

h,k,l – Miller indexes

d – d-spacing, nm

An average grain sizes of coatings (shape factor) has been calculated using Debye-Sherrer formula:

$$\mathcal{T} = \frac{k\lambda}{\beta\cos(\theta)},\text{ where}$$

Т - is the mean size of the ordered (crystalline) domains, which may be smaller or equal to the grain size

k – shape factor (0,9)

λ – X-Ray wavelength (1,5418 nm for copper tube), nm

β – line broadening at half the maximum intensity (FWHM), radians

Ө - Bragg angle, radian.

The Debye-Scherrer equation is limited to nano-scale particles. It is not applicable to grains larger than about 0.1 μm. It is important to realize that this formula provides a lower bound on the particle size. The reason for this is that a variety of factors can contribute to the width of a diffraction peak; besides crystallite size, the most important of these are usually inhomogeneous strain and instrumental effects. If all of these other contributions to the peak width were zero, then the peak width would be determined solely by the crystallite size and the Debye-Scherrer formula would apply. If the other contributions to the width are non-zero, then the crystallite size can be larger than that predicted by calculations, with the "extra" peak width coming from the other factors.

For analyzing the surface morphology and chemical composition, SEM microscopy (Philips XL-30) equipped with a field emission gun at accelerating voltage of 10 kV) was performed. Heretofore, by evaporation technique, non-conductive samples (CeO_2) had been covered with 100 nm carbon layer.

## 2.5 Static test with liquid gallium

Solid gallium is a blue-gray metal with orthorhombic crystalline structure; very pure gallium has a stunning silvery color (Fig.2.10). The density at 20°C is 5,1 g/cm^3 , melting and boiling points are 29,8 and 2204°C correspondingly (one of the largest liquid range for metals).

Fig.2. 10 Crystalline gallium

The thermal conductivity of liquid gallium is quite low 40,6 W/mK (300K), which could be explained by the fact that in a liquid state gallium exist as a biatomic covalent compound – Ga_2 dimers. This also explains the drop of the melting point compared to its neighbour elements aluminium and indium.

Liquid gallium possesses enormous surface tension, which few times exceeds the value for mercury. This has been studied by many scientists (Fig. 2.11). The scatter in the gallium surface tension data is widely attributed to the presence of trace concentrations of surface active impurities in the different measurement[38,39,40,41,42,43].
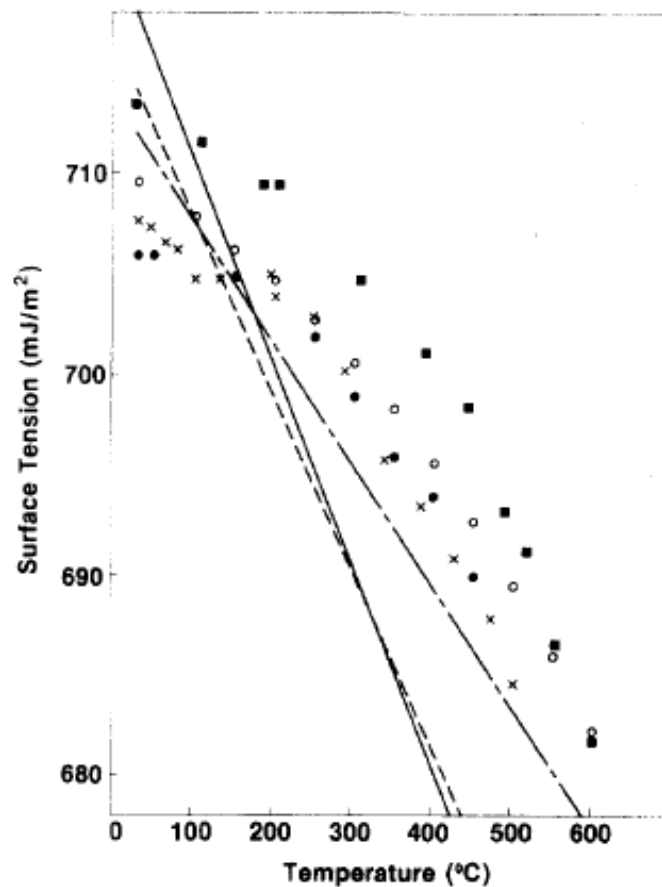
Fig.2. 11 Summary of measurements of the surface tension of gallium

Ga has a low vapor pressure at high temperatures (unlike mercury) (Table 2.2), which is a big advantage for usage this metal as a coolant:

Table 2. 2 Gallium vapor pressure at different temperatures

P/Pa	1	10	100	1 k	10 k	100 k
at T/K	1310	1448	1620	1838	2125	2518

At room temperature, gallium metal is unreactive towards air and water due to the formation of a passive, protective oxide layer. At higher temperatures, however, it reacts with oxygen in the air to form gallium(III) oxide, Ga_2O_3[44]. Reducing Ga_2O_3 with elemental gallium in vacuum at 500 °C to 700 °C yields the dark brown gallium(I) oxide, Ga_2O[45]. Ga_2O is a very strong reducing agent, capable of reducing H_2SO_4 to H_2S. It disproportionates at 800 °C back to gallium and Ga_2O_3[46]. The crystal structure of gallium oxide clusters was studied elsewhere[47].

The phase diagram Ga-O is displayed below[48]:
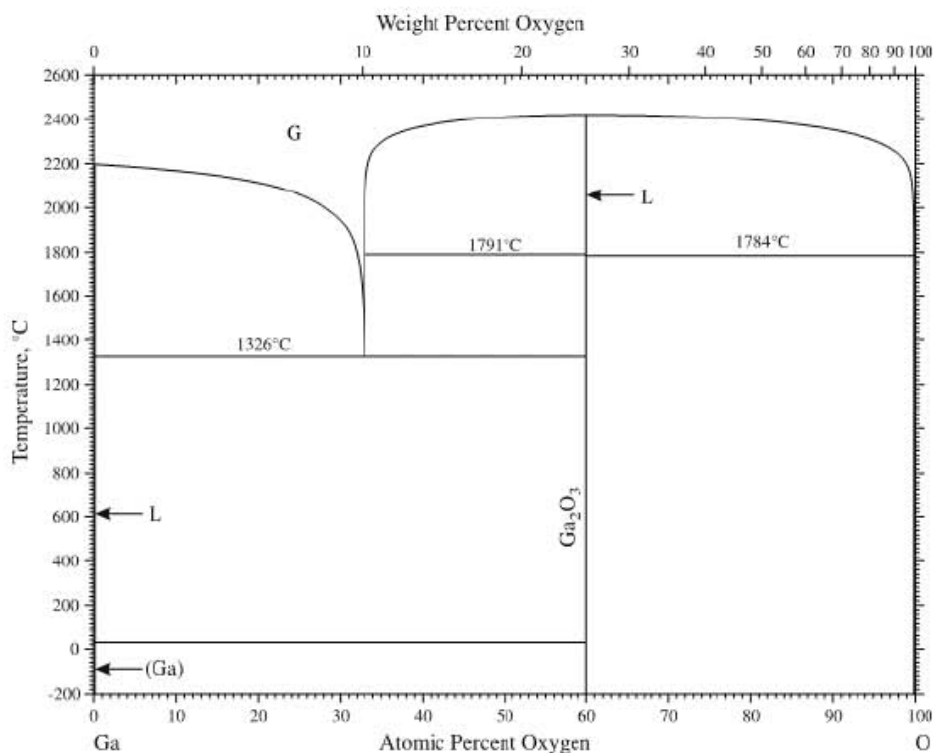
Fig.2. 12 Ga-O phase diagram

Gallium attacks most other metals by diffusing into their metal lattice. Gallium, for example, diffuses into the grain boundaries of Al/Zn alloys[49] or steel[50], making them very brittle. Also,

gallium metal easily alloys with many metals, and was used in small quantities as a plutonium-gallium alloy in the plutonium cores of the first and third nuclear bombs, to help stabilize the plutonium crystal structure[51].

The wettability and contact interaction of gallium with various surfaces has been studied extensively. The wettability of sapphire, quartz and graphite by gallium, gallium-based binary alloys with indium, tin, copper, silver, nickel, manganese, chromium, vanadium and titanium and by ternary Cu-Ga-Ti, Cu-Ga-Cr and Cu-Ga-Mn alloys has been studied by sessile drop, plate weight and meniscus form methods. The character and intensity of contact reactions and the composition of transition layers at the solid-melt boundary have been investigated by X-ray analysis and profilographic measurements and the correlation between the wettability and the contact reaction intensity has been established. The condition for high wettability of non-metallic solids by multicomponent melts is shown to be a combination of high affinity of a component for solid phase atoms with high thermodynamical activity of this component in the melt[52].

Within the bounds of this project, the test of obtained coatings was performed by simply visual observations of Ga interaction with the surfaces of obtained coatings at different temperatures. As it was described above, on air gallium forms an oxide layer on its surface, so we must keep in mind that during the experiment we had not only Ga-surface but mainly Ga_2O_3-surface interaction. In fact, it was calculated that the surface of gallium, exposed to air environment, oxidizes and consist of approximately 85% of oxides on the surface (Fig. 2.13)[51]. Also qualitatively this is what might have been expected from the imaging experiments, which illustrate that 88% of the Ga surface is covered with oxide[53].
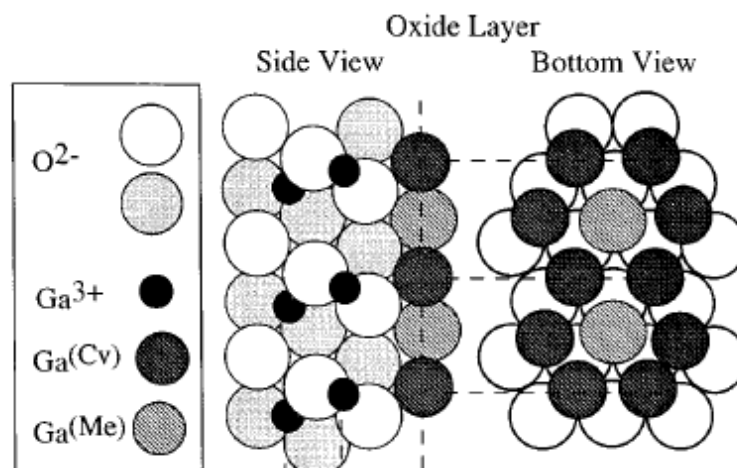
Fig.2. 13 Proposed atomic arrangement in the oxide layer, with atomic diameters of 2.64 Å for O^{2-}, 1.24 Å for Ga^{3+}, 2.44 Å for covalent (Cv) Ga, and 2.50 Å for metal (Me) Ga

In our experiment sputtered coatings on aluminum substrate were placed in glass Petri dish on the heater. By the use of plastic pipette, the drop of liquid gallium was placed on tested surface. The interaction was observed at room temperature (22 ˚C), 50˚C, 100˚C and 200˚C. The temperature was measured by infra red thermometer (Fig. 2.14). After that the drop was removed from the surface and samples were visually analyzed.

Fig.2. 14 Experimental set-up for static liquid gallium test

After static test is performed, the test in dynamic conditions should be done. The model of cooling system should be consisted of coated tubes, gallium container and Teflon pump. In this case we will have a refreshed gallium flow all the time and thus no problem with oxidation. And hereby this test will be me more accurate.

CHAPTER 3. DIAMOND-LIKE CARBON THIN FILMS

3.1 THEORETICAL BACKGROUND

3.1.1 Structure

Diamond-like carbon (DLC) exists in seven different forms of amorphous carbon materials that display some of the typical properties of diamond. All forms contain significant amounts of sp^3 hybridized carbon atoms. The reason that there are different types is that even diamond can be found in two crystalline polytypes. The usual one has its carbon atoms arranged in a cubic lattice, while the very rare one (lonsdaleite) has a hexagonal lattice. By mixing these polytypes in various ways at the nanoscale level of structure, DLC coatings can be made that at the same time are amorphous flexible, and yet purely sp^3 bonded "diamond". The hardest, strongest, and slickest is such a mixture, known as tetrahedral amorphous carbon, or *ta-C* (Fig.3.1).

In those cases cubic and hexagonal lattices can be randomly intermixed, layer by atomic layer, because there is no time available for one of the crystalline geometries to grow at the expense of the other before the atoms are "frozen" in place in the material. Amorphous DLC coatings can result that have no long-range crystalline order. Without long range order there are no brittle fracture planes, so such coatings are flexible and conformal to the underlying shape being coated, while still being as hard as diamond[54].
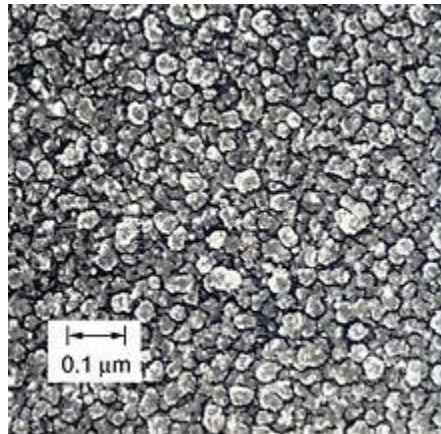
Fig.3. 1 SEM image of a gold-coated ta-C coating

As we see from Fig.3.1, structural elements are not crystallites but are nodules of sp^3-bonded carbon atoms where lattice geometries randomly alternate between the cubic and hexagonal polytypes of diamond.

That "pure" DLC material is *ta-C* and others are approximations that are degraded by diluents such as hydrogen, sp^2 bonded carbon, and metals.

3.1.2 Obtaining

Several methods have been developed for producing diamond-like carbon films:

- filtered cathodic arc deposition

- primary ion beam deposition of carbon ions (IBD)

- sputter deposition of carbon with or without bombardment by an intense flux of ions (Physical Vapour Deposition or PVD)

- deposition from an RF plasma, sustained in hydrocarbon gases, onto substrates negatively biased (Plasma Enhanced Chemical Vapour Deposition or PECVD)

- IDECR (Integrated Distributed Electron Cyclotron Resonance) using acetylene-oxygen plasma

It is known that in sputtering, sp^3 bonding of DLC is promoted by deposition from a source of medium-energy ions[55]. At present, the most highly sp^3 bonded form of α-C has been deposited from a filtered beam of C^+ ions[56,57]. The ion filtering leads to deposition from a relatively monoenergetic beam of a single ion species. The resulting α-C has been found to contain up to 80-85% of tetrahedrally bonded sp^3 C sites[58,59]. A similar form was proposed by the laser ablation of graphite[60,61].

Much of the work on DLC has been carried out on α-C:H prepared by plasma-enhanced chemical vapor deposition of hydrocarbon gasses[62]. Plasma deposition has so far produced rather less sp^3 bonded and less diamondlike films. The lower sp^3 content presumably arises because the ionization of the deposition is quite low[63]. This suggests that a more diamondlike form of α-C:H could be deposited by increasing the ionization of the deposition flux[64].

It is well-known that the decomposition of hydrocarbons in plasma depends strongly on source gas, the operation pressure and the gas flow rate[65]. Usually, hydrocarbon plasmas can exhibit a wide spectrum of C_xH_y radicals in an ionized or neutral state. The plasma composition depends on the various chemical pathways in the plasma, and these depend on plasma parameters such as electron temperature, electron density and degree of ionization.

3.1.3. Properties

Amorphous (a-C) and hydrogenated amorphous carbon (a-C:H) films have high hardness, low friction, electrical insulation, chemical inertness, optical transparency, biological compatibility, ability to absorb photons selectively, smoothness, and resistance to wear. For a number of years, these economically and technologically attractive properties have drawn almost unparalleled

interest towards these coatings. Carbon films with very high hardness, high resistivity, and dielectric optical properties, are now described as diamond-like carbon or DLC, *Table 3.1*.

Table 3. 1 Properties of diamond and DLC materials

Property	Thin Film			Bulk	
	CVD Dia.	a-C	a-C:H	Diamond	Graphite
Crystal Structure	Cubic	Amorphous	Amorphous	Cubic	Hexagonal
	$a=3.561\text{Å}$	sp^3/sp^2	sp^3/sp^2	$a=3.567\text{Å}$	$a=2.47\text{Å}$
Form	Faceted crystals	Smooth or rough	Smooth	Faceted crystals	Hexagonal
Hardness (H_v)	3000-12000	1200-3000	900-3000	7000-10000	-
Density (g/cm^3)	2.8-3.5	1.6-2.2	1.2-2.6	3.51	2.26
Refractive Index	-	1.5-3.1	1.6-3.1	2.42	2.15
Electrical Resistivity (Ω/cm)	$>10^{13}$	$>10^{10}$	10^6-10^{14}	$>10^{16}$	0.4
Thermal Conductivity ($W/m^.K$)	1000-2000	-	-	2000	3500
Chemical Stability	Inert	Inert	Inert	Inert	Inert
Hydrogen Content (H/C)	-	-	0.25-1	-	-
Growth Rate ($\mu m/hr$)	~1	2	5	1000 (synthetic)	-

3.1.4 Application

Applications of DLC typically utilize the ability of the material to reduce abrasive wear. Tooling components, such as endmills, drill bits, dies and molds often use DLC in this manner. DLC is also used in the engines of modern supersport motorcycles. Virtually all of the multi-bladed razors used for wet shaving have the edges coated with hydrogen-free DLC to reduce friction, preventing abrasion of sensitive skin. The implantable human heart pump can be considered the ultimate biomedical application where DLC coating is used on blood contacting surfaces of the key components of the device[66].

3.2 EXPERIMENTAL PART

3.2.1 Obtaining and analyses of DLC coatings

In this project DLC coatings were prepared by Hollow Cathode Magnetron Sputtering described in Chapter 2.2. The sample holder with three spirally assembled quartz samples was vertically inserted in the HC chamber and fixed (Fig.2.6, 2.7). After base vacuum was reached (10E-6 mbar), the inductive coil was placed around the chamber (I_{DC}=2A), acetylene container was connected to the inlet on the top of the chamber, and after that the RF power was applied via a capacitors and matching network. Depositions lasted for 10 and 15 min.

The presence of external magnetic field (copper coil) is necessary in our case, because it maximizes plasma ionization and confines the plasma along the hollow cathode surface. A low pressure also has the advantage of minimizing ion collisions, so that the plasma beam is relatively monoenergetic.

As a precursor for DLC, *acetylene* was used in the present work because of its relatively simple dissociation pattern. The plasma decomposition of a molecule can be described in terms of electron-molecule (primary) or ion-molecule (secondary) collisions, and their associated rate coefficients or their related appearance potentials[67]. It has been shown that the dissociation of acetylene is dominated by its ionization at an appearance potential of 11,2 eV. In contrast, other processes leading to C-C bond breaking or polymerization require appearance potentials over 17 keV. Acetylene is unique among the hydrocarbons in having such a well-defined reaction path. It contrasts with alkanes and alkenes, whose appearance potentials do not show such a distinction. Also using acetylene, DLC coating is expected to have low hydrogen contain which is important for mechanical properties of obtained film[63] *(Table 3.1)*.

The films were sputtered in HC vacuum chamber; deposition parameters such as bias potential, different gas flow and working pressure were investigated, analyzed and displayed in *Table 3.2*. In case of additional argon flux, after base pressure in the chamber was reached, the Ar flow was set and controlled by flow meter; then acelylene flow was set just by leak valve until we reached a desirable total pressure.

Table 3. 2 Deposition parameters for DLC coatings

Sample, №	RF power, W	Coil current, A	DC bias tension, V	DC Bias current, mA	Base pressure, mbar	Working pressure, mbar	Gas flux	Deposition time, min
13	200	2	160	35	2x10E-5	2,0x10E-3	C_2H_2	10
14			200	45		2,0x10E-3	C_2H_2	
15			200	144		7,5x10E-4	C_2H_2	
16			200	53		3,2x10E-3	C_2H_2, Ar(1,2sccm)	
17			200	24		7,3x10E-3	C_2H_2	
24	200	2	200	43	2x10E-5	3,1x10E-3	C_2H_2, Ar(1,2sccm)	15
20			200	45		3,9x10E-3	C_2H_2, Ar(5,0sccm)	
21			200	44		2,5x10E-3	C_2H_2, Ar(5,0sccm)	
22			200	45		3,5x10E-3	C_2H_2, Ar(10,0sccm)	
23			200	42		5,8x10E-3	C_2H_2, Ar(10,0sccm)	
26	200	2	80	26	2x10E-5	2,5x10E-3	C_2H_2, Ar(1,2sccm)	15
27			50	49		2,9x10E-3	C_2H_2, Ar(1,2sccm)	
28			80	16		3,6x10E-3	C_2H_2, Ar(1,2sccm)	

Obtained coatings were not hard, had different color varying from yellow to black (Fig. 3.2) and quite a different thicknesses (*Table 3.3*). Some of them were stressed probably due to overcoming the thickness threshold caused by internal stresses due to electron bombardment or if quartz samples were not clean enough. It should be mentioned that substrate cleaning by plasma discharge should be performed before deposition.

After each deposition, we got 3 quartz samples, mentioned below as 1 (top), 2 (middle), 3 (bottom).
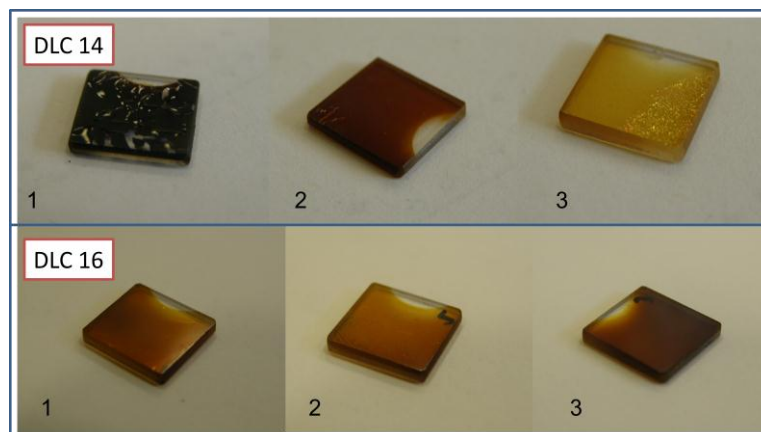
Fig.3. 2 DLC coatings on quartz substrate

Table 3. 3 Thickness of obtained DLC coatings

Sample, №	Thickness of quartz samples at different position on sample holder, nm		
	Top (1)	Middle (2)	Bottom (3)
13	7500	3400 (stressed)	1000
14	10500 (stressed)	5200	1200(stressed)
15	stressed	stressed	stressed
16	2200	2600	2800
17	8300	3000	800
20	200	not detectable	
24	3245	4738	3421
21	200	-	-
23	600	-	-
26	570	1500	850
28	5000	2000	8000

Quartz samples (16) have similar thickness and color, it differs this experiment conditions from others. In this case the process was supplied with argon flux of 1,2 sccm as well as with acetylene (Fig.3.2).

To understand the role of argon in this process we repeated experiment 16 (sample №24 *Table 3.2*) and carried out the same deposition but every time increasing the argon flux (samples 20-23, Fig.3.3a). Experiment 16 was reproducible – coatings had similar color and thickness, but they still were not hard. Increasing Ar flux caused formation of thinner and more transparent coatings (Fig.3.3), which still didn't possess mechanical hardness and chemical inertness.
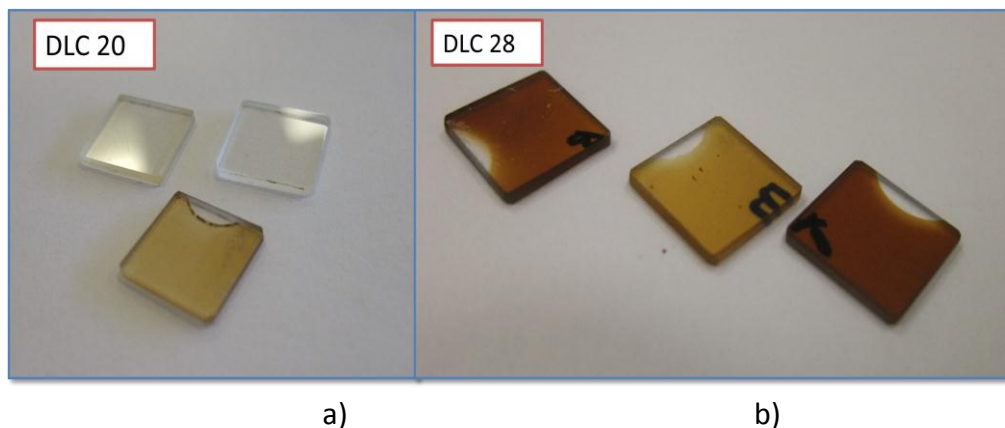
Fig.3. 3 DLC samples: a) increased Ar flux (5 sccm), b) decreased bias (80 V)

To enhance the most promising coating (exp. №16), we repeated this deposition changing bias tension (samples 26-28). But it didn't improve film properties (Fig. 3.3b). Moreover, it is well-known that the influence of ion bombardment of growing DLC films is very important for obtaining hard coatings. So as we expected, decreased bias potential didn't improve quality of our films.

We suppose that along with chemical vapor deposition of acetylene, sputtering of carbon from cathode surface occurs in an uncontrollable way. Additional argon flux caused probably sputtering of carbon and thereby decreasing CVD of acetylene which is very important for DLC formation. C_2H_2 was supplied from the top of the chamber causing pressure gradient along the sample holder which explains thickness variations of samples along the axis of hollow cathode.

3.2.2. Test with liquid gallium

Suitable DLC coating on aluminum was not obtained; hence the test against liquid gallium embrittlement was not performed.

3.3 CONCLUSIONS

In frames of this project, satisfactory DLC coatings were not obtained. It happened due to many reasons, for example, pressure gradient, electron bombardment of growing film, uncontrolled carbon sputtering from the cathode etc.

The sputtering system for DLC should be improved in order to obtain even coatings along the sampleholder. For this purpose it is possible to reconstruct the acetylene inlet – for example, to be presented like "shower injection", in order to have the same gas distribution along the axis of the hollow cathode. Electron collecting grids should be installed, and then electron bombardment of growing film will be reduced. The carbon cathode could be replaced by inert one, and after that the properties of DLC coating, obtained only by plasma assisted chemical vapor deposition, could

be performed. DLC coatings could be also obtained by DC sputtering of carbon hollow cathode using (along with argon) hydrogen as a reactive gas.

It is necessary to analyze the structure of obtained DLC coatings. SEM microscopy could be used in order to see the cross-section of growing film. By Raman and Infrared spectroscopy we could identify sp^2 and sp^3 bonds and their ratio. After that the deposition parameters such a pressure, gasses fluxes, substrate temperature, bias tension, power, time, could be optimized.

CHAPTER 4. NIOBIUM THIN FILMS

4.1 THEORETICAL BACKGROUND

4.1.1 Structure

Niobium is a transition metal, which is often found in the pyrochlore mineral. The element is placed in group 5 of the periodic table, although it has an atypical configuration in its outermost electron shells compared to the rest of the members. It has a body-centered structure.
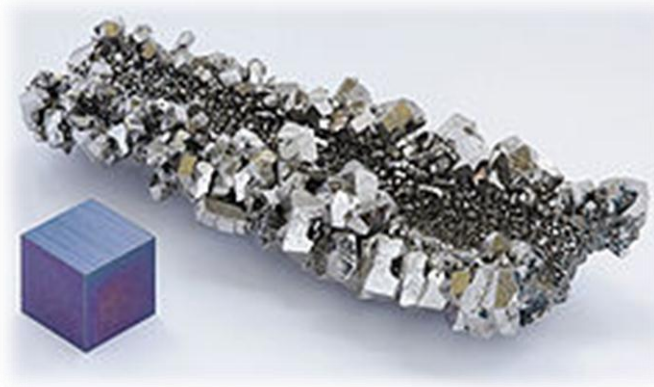
Fig.4. 1 Niobium crystal and 1 cm^3 Nb cube

4.1.2 Obtaining

Niobium can be obtained from ores rich of its oxides. After separation from other minerals (mostly tantalum oxide), niobium pentaoxide is reduced to metallic niobium.

Niobium thin films can be deposited by magnetron sputtering which is well described. The DC bias sputtered Nb films have the best quality and properties. This deposition technique requires 300-500 ˚C substrate temperature, 1 kW cathode discharge and -120 V bias tension. Obtained coatings have 2000 nm thickness, appropriate structure and properties[68].

4.1.3 Properties

Niobium is lustrous, grey, ductile, paramagnetic metal (Fig. 4.1). It becomes a superconductor at cryogenic temperatures. At atmospheric pressure, it has the highest critical temperature of the elemental superconductors: 9.2 K[69]. Niobium has the largest magnetic penetration depth of any element. The superconductive properties are strongly dependent on the purity of the niobium metal. When very pure, it is comparatively soft and ductile, but impurities make it harder[70].

Some physical properties are collected in Table 4.1:

Table 4. 1 Physical constants for niobium

Property	Value, units
Density	8,57 g/cm^3
Melting point	2477 ˚C
Boiling point	4744 ˚C
Electrical resistivity	15,2 μΩ.m
Thermal conductivity (RT)	53,7 W/(mK)
Thermal expansion	7,3 μm/(mK)
Mosh hardness	6

The metal takes on a bluish tinge when exposed to air at room temperature for extended periods. The color depends on formed oxides thickness.

Despite presenting a high melting point in elemental form (2,468 °C), it has a low density in comparison to other refractory metals. Furthermore, it is corrosion resistant, exhibits superconductivity properties, and forms dielectric oxide layers.

Niobium is slightly less electropositive and more compact than its predecessor in the periodic table, zirconium, whereas it is virtually identical in size to the heavier tantalum atoms, owing to the lanthanide contraction. As a result, niobium's chemical properties are very similar to those for tantalum, which appears directly below niobium in the periodic table[71]. This is the reason of difficulties to separate tantalum and niobium.

4.1.4 Application

Niobium is used mostly in alloys, the largest part in special steel such as that used in gas pipelines. Although alloys contain only a maximum of 0.1%, that small percentage of niobium improves the strength of the steel. The temperature stability of niobium-containing superalloys is important for its use in jet and rocket engines. Niobium is used in various superconducting materials. These superconducting alloys, also containing titanium and tin, are widely used in the superconducting magnets of MRI scanners. Other applications of niobium include its use in welding, nuclear industries[72] (it has a low capture cross-section for thermal neutrons[73]), electronics, optics, numismatics and jewelery. In the last two applications, niobium's low toxicity and ability to be colored by anodization are particular advantages.

It is estimated that out of 44,500 metric tons of niobium mined in 2006, 90% was used in the production of high-grade structural steel, followed by its use in superalloys[74].

Niobium-germanium (Nb_3Ge), niobium-tin (Nb_3Sn), as well as the niobium-titanium alloys are used as a type II superconductor wire for superconducting magnets[75]. These superconducting magnets are used in magnetic resonance imaging and nuclear magnetic resonance instruments as well as in particle accelerators. The Superconducting Radio Frequency (RF) cavities used in the free electron lasers TESLA and XFEL are made from pure niobium[76].

The high sensitivity of superconducting niobium nitride bolometers make them an ideal detector for electromagnetic radiation in the THz frequency band.

Niobium also is used as a precious metal in commemorative coins, often with silver or gold.

Nb posess inertness and relatively good corrosion resistance, that's why we are considering this metal as a possible protective barrier against LME.

4.2 EXPERIMENTAL PART

4.2.1 Obtaining and analyses of Nb coatings

Niobium coatings onto aluminum were obtained by DC magnetron sputtering (Chapter 2.3). All samples had typical niobium color and were reflective (Fig.4.2).

Fig.4. 2 Obtained niobium coating at 22 ˚C substrate temperature

The deposition parameters for niobium films are described in *Table 4.2*.

Table 4. 2 Deposition parameters for niobium coatings

Sample, №	Substrate temperature, ˚C	Ar flux, sccm	DC current, A	DC tension, V	Base pressure, mbar	Target-substrate distance, cm	Time, min
1-3	22	8	0,5	340	2,0x10E-5	6,5	30
4	floating*			330		7,5	30

* by term ***floating temperature*** we mean that during the deposition, the substrate was neither heated nor water cooled. The increasing of substrate temperature was caused by the sputtering process itself

Niobium coating, obtained at floating temperature, had lattice parameter a bit higher than standard (*Table 4.3*) and lower sputtering rate due to heating of the substrate and longer distance from the target to the sample holder.

It should be also mentioned that sometimes the compressive stress is preferential for sputtered coatings, but we can't say this about tensile stress which causes delamination and peeling. Indeed, to find the right compromise is very difficult.

Table 4. 3 Parameters for obtained Nb films

Sample, №	Thickness , nm	Deposition rate, nm/sec	Cubic lattice parameter, Å	Average grain size, Å
Nb standard	-	-	3,3000	-
2	1600	0,8889	3,3006	165
4	1400	0,7794	3,3155	195

All coatings, obtained at different temperatures, were adhesive to aluminum and quartz substrates. Before deposition of Nb (№4), the substrate was firstly cleaned by plasma discharge. For such films, an average grain size calculated with Debye-Schrerrer formula is bigger than for coatings, deposited on water cooled substrate.

On Fig. 4.3 we see the morphology of Nb coating obtained at room temperature:
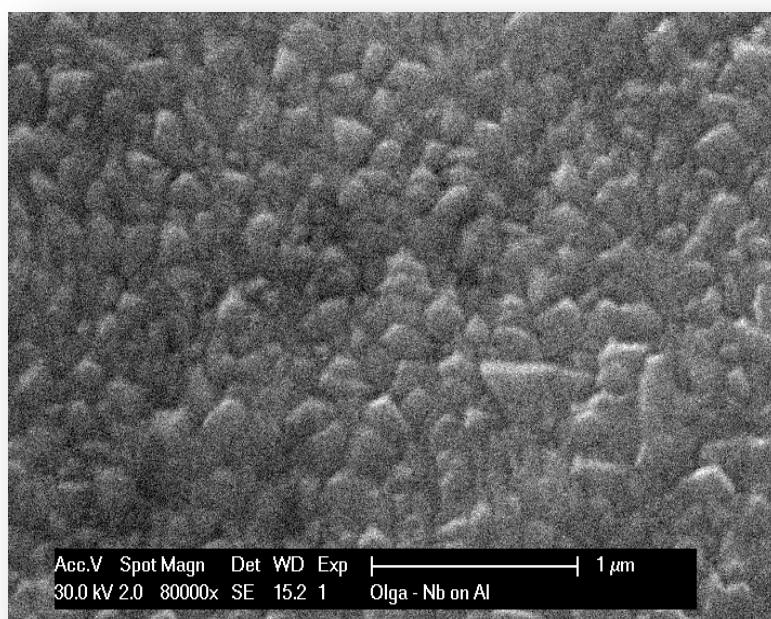
Fig.4. 3 SEM micrograph of Nb coating obtained at room temperature

XRD spectrums of Nb coatings were obtained and analyzed. All peaks were in agreement with characteristic Nb spectrum (Fig.4.4).
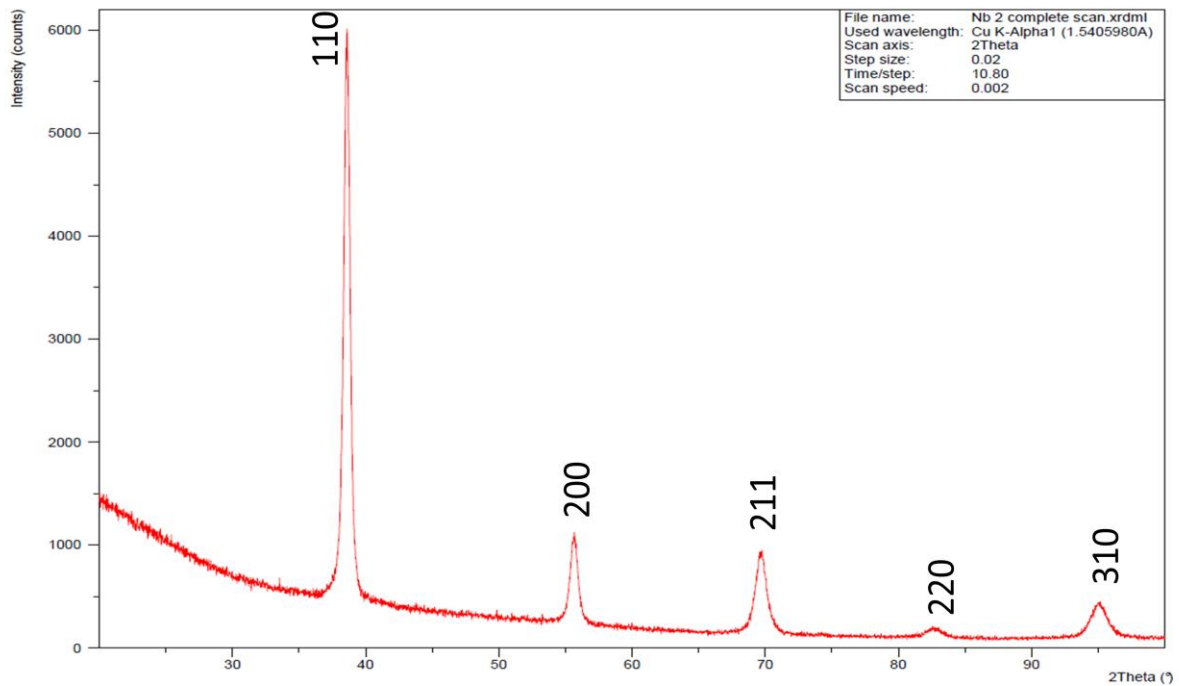
Peak list

No.	h	k	l	d [A]	2Theta[deg]	I [%]
1	1	1	0	2.33789	38.475	100.0
2	2	0	0	1.65322	55.542	16.0
3	2	1	1	1.34993	69.587	20.0
4	2	2	0	1.16882	82.454	5.0
5	3	1	0	1.04560	94.903	4.0
6	2	2	2	0.95456	107.602	1.0
7	3	2	1	0.88379	121.286	4.0
8	4	0	0	0.82664	137.447	1.0

Fig.4. 4 XRD spectrum of Nb coating

4.2.2 Test with liquid gallium

Liquid gallium wets Nb coatings obtained at high substrate temperature and leaves traces on coatings obtained at room temperature (Fig. 4.5 a, b). We can see that niobium film (Fig. 4.5 b) got yellowish color after heating. Probably niobium oxides and nitrides were formed.

Nevertheless, no embrittlement was observed even after continuous heating at 200 ˚C. It was shown that wettability of niobium by liquid gallium is higher for films obtained at high temperatures (floating, 200 ˚C). It is probably connected to increased crystallinity level and improved grain boundary connectivity, in-between which the penetration of Ga occurs.

We suppose that Ga partly penetrates through the grain boundaries of the film but corrosion stops probably due to Ga_2O_3 formation on the surface.
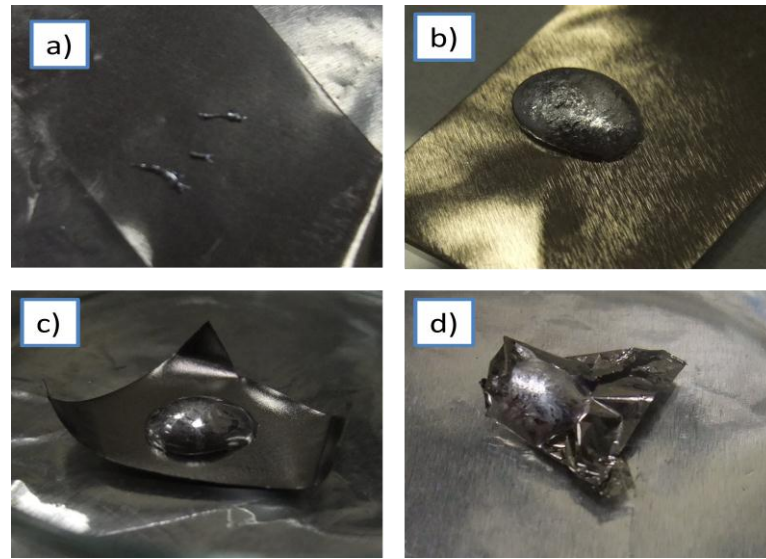
Fig.4. 5 Interaction of Ga with Nb: coatings obtained at 22 ˚C substrate temperature, b) at floating temperature, c) bulk niobium, d) niobium foil (rolled, 0,01 mm thick)

Also for comparison, the interaction of liquid gallium with bulk niobium and niobium foil were investigated (Fig.4.5 c, d). Both these materials were wet by gallium but didn't corrode inwards as well.

4.3 CONCLUSIONS

Niobium thin films were obtained, characterized and tested against liquid metal embrittlement.

For all experiments depostition parameters were kept the same (base pressure 10E-5, current 0,5A, 8 sccm Ar flux), only substrate temperature was a varying parameter. Thus, Nb films obtained at floating or high (200 ˚C) substrate temperature, had rather higher wettability (visually observed but not measured) by liquid gallium that films obtained at 22 ˚C.

It was found from XRD spectrums that increasing substrate temperature; we increase the crystallinity of the coating which probably makes easier gallium penetration into the film. In author's opinion, when liquid gallium is placed on the coating, oxygen, which is located between these grain boundaries, forms gallium oxides and these oxides block further penetration of gallium in our coatings.

All obtained coatings are wet by gallium but visually we didn't observe the embrittlement.

CHAPTER 5. NIOBIUM NITRIDE THIN FILMS

5.1 THEORETICAL BACKGROUND

5.1.1 Structure

Niobium nitride is a grey-yellowish solid compound with body centered cubic structure (Fig.5.1). The NbN system is complex and presents various phases, e.g., β, δ, ε, γ, δ´ and η[77]. The well studied phase remains the cubic δ phase.

δ´-NbN   β-Nb₂N   δ-NbN

● N
○ Nb
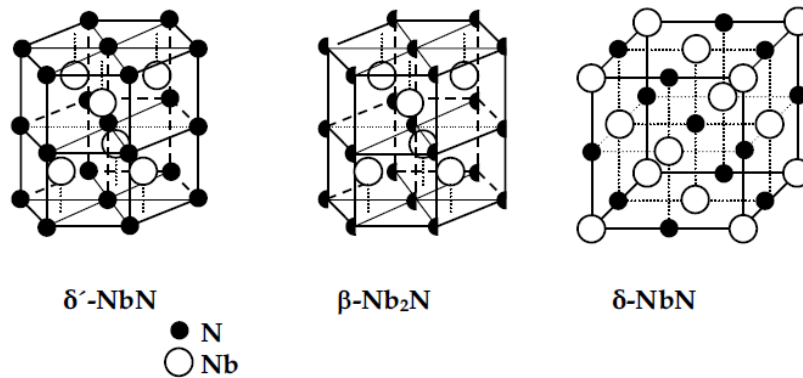
Fig.5. 1 Elementary cell of crystalline structure of Nb-N phases: hexahonal δ'-NbN, β-Nb$_2$N and cubic δ-NbN respectively. For the β-Nb$_2$N notation means that only half of the nitrogen sites are occupied[78]

5.1.2 Obtaining

The NbN films have been mostly grown employing Physical Vapor Deposition (PVD) techniques, including pulsed laser deposition[79], molecular beam epitaxy[80], and reactive sputtering[81,82]. On the other hand, one should pay more attention to NbN thin film growth by chemical vapor deposition (CVD), a method distinguished from the PVD by rather simple apparatus, high flexibility of the deposition process, better step coverage, higher growth rate etc. NbN films tend to grow at high temperatures (800-1000°C), which appears to be a disadvantage of the thermally activated, conventional CVD[83]. Nevertheless, creating a plasma discharge in the reactor can significantly simplify the deposition[84]. Due to the fact that nitrogen plasma contains partially ionized and dissociated molecules the processing temperature, in many cases, can be kept lower. The choice of precursor is also important: while organometallic precursors such as Nb dialkylamides and alkylimides have been shown to be suitable for deposition of NbN by thermal and plasma CVD at low temperatures, contamination by carbon and especially hydrogen appear to be unavoidable. Radio frequency (RF) nitrogen plasma induced CVD has been also applied to grow superconducting NbN thin films using $NbCl_5$ as a precursor.

5.1.2 Properties

The density of NbN is 8,47 g/cm^3 and melting point is 2573 ˚C. Niobium nitride posess extraordinary mechanical and chemical stability[85], NbN films feature relatively high critical temperature, critical fields, critical current densities[86].

5.1.3 Application

Niobium nitride's main use is as a superconductor. Detectors based on it can detect a single photon in the 1-10 micrometer section of the infrared spectrum, which is important for astronomy and telecomunications. It can detect changes up to 25 gigahertz. Niobium nitride is also used in absorbing anti-reflective coatings.

Superconducting niobium nitride films prepared by reactive DC mgnetron sputtering are used as a material for superconducting cavities. The main advantages in this case are: law secondary electron emission coefficient[87], good immunity against radiation and chemical agents and less serration in oxidation than niobium, indicating less RF residual losses and higher RF breakdown fields[88]. Moreover, thermal breakdown due to the quenching of certain microscopic regions from the superconducting state to the normal state is reduced thanks to the high transition temperature. Finally, NbN exhibits lower RF losses than Nb, at the same temperature[89].

5.2 EXPERIMENTAL PART

5.2.1 Obtaining of NbN coatings

Niobium nitride coatings were obtained by reactive DC magnetron sputtering as described in chapter 2.3. General deposition parameters are collected in the *Table 5.1*:

Table 5. 1 Deposition parameters to obtain NbN coating

Base pressure, mbar	DC current, A	Substrate temperature, ˚C	Ar flux, sccm	N$_2$ flux, sccm	Time, min
2x10E-5	0,5	22 floating temp. 200 500	8	4,0..5,5 5,1	30

To find the optimal nitrogen flux for deposition at room temperature (22 ˚C), the following experiment had been carried out. At constant DC current (0,5 A) and fixed argon flow (8 sccm), the

sputtering was performed (base pressure 2,18E-5 mbar). During the deposition the nitrogen flux was changed in the range 0-9,5 sccm with step 0,5 and in the range 10-16 with step 1 sccm. Corresponding total pressure and voltage of the system were detected (*Table 5.2*).

Table 5. 2 Data for experiment to find optimal N_2 flux to obtain NbN film (22 ˚C, 8 sccm Ar flux)

Nitrogen flux, sccm	Total pressure, mbar	Tension, V
0	4,1	335
2	4,8	329
2,5	5,2	328
3	5,5	327
3,5	5,7	325
4	6,0	324
4,5	6,3	327
5	6,5	367
5,5	7,0	387
6	7,3	393
6,5	7,7	398
7	8,1	406
7,5	8,6	410
8	8,9	412
8,5	9,2	415
9	9,6	416
9,5	10,0	420
10	10,3	421
11	11,2	424
12	11,9	429
13	12,8	431
14	13,5	434
15	14,4	436
16	15,4	438

After that, the graphs of nitrogen flux vs total pressure and nitrogen flux vs voltage were plotted:
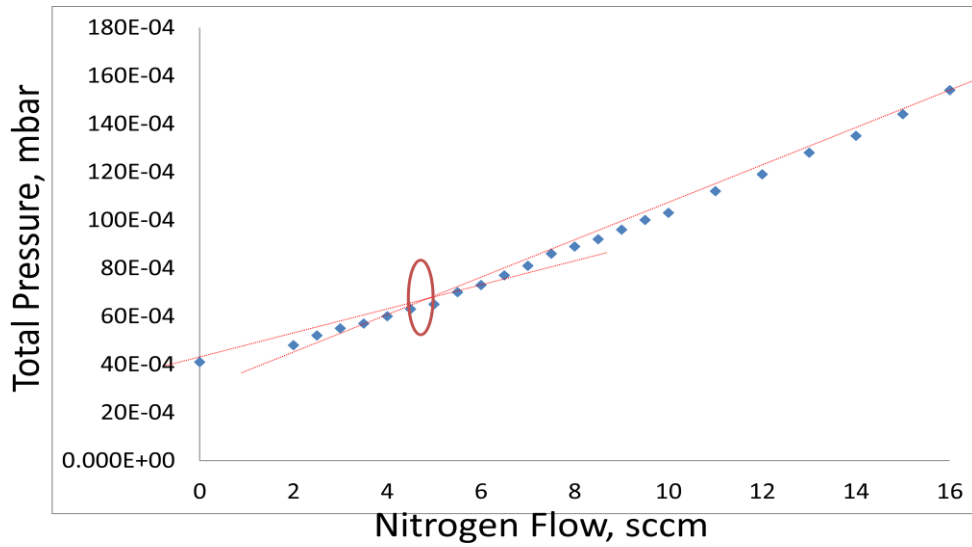
Fig.5. 2 Total pressure of the system versus nitrogen flow during sputtering
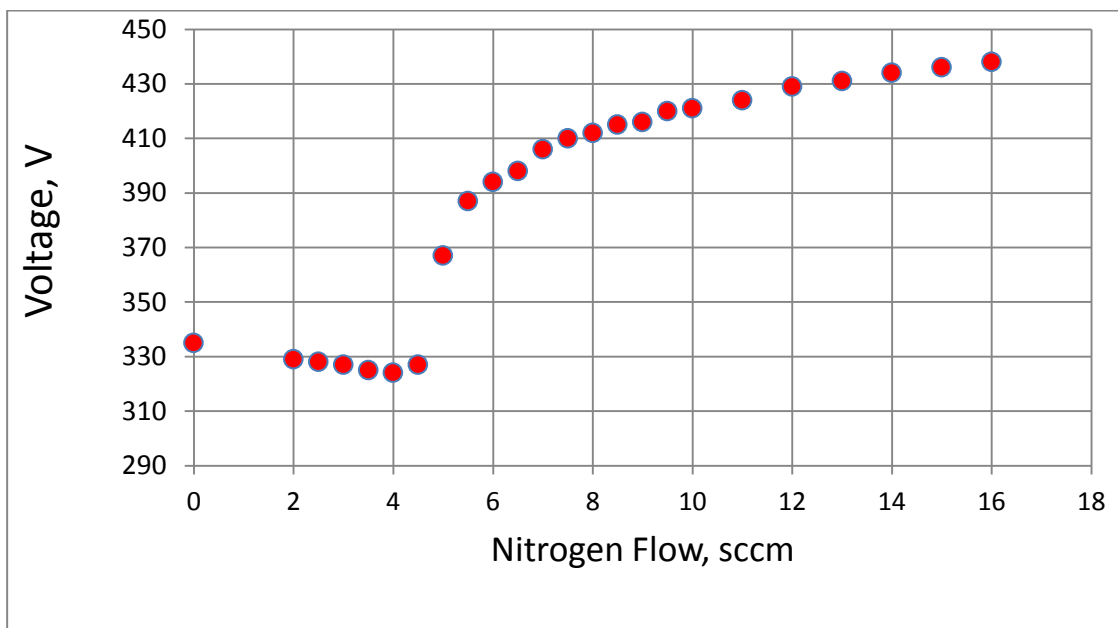
Fig.5. 3 Voltage versus nitrogen flow during sputtering

On Fig. 5.2 we can see that increasing nitrogen pressure we increased the total pressure of the system. But at N_2 flow around 5 sccm, a little pressure drop was observed and after this point the total pressure increased again almost linearly. We can conclude, that optimal nitrogen flow for sputtering must be in range of 4,0-5,5 sccm for deposition at 22 ˚C. In this region nitrogen is used to form niobium nitride film, above it we have excess of nitrogen, below – understochiometric conditions.

Data shown in Fig. 5.3 confirm this information. Thus the voltage drop around N_2 flow 5 sccm shows the optimal gas flow composition, where the film is "pumping". At higher nitrogen flux, there is the excess of N_2 gas and its ionization takes place.

After that the reactive sputtering of NbN films at N_2 flux 4,0…5,5 sccm was performed. Deposition parameters are displayed in *Table 5.3*.

Table 5. 3 Deposition parameters for sputtering deposition of NbN films at room temperature

Sample, №	Substrate temperature, ˚C	Nitrogen flux, sccm	Argon flux, Sccm	DC current, A	DC tension, V	Base pressure, mbar	Target-substrate distance, cm	Deposition time, min
1		4			405			
13		4,5						
17		4,9			368			
4		5,0			390			
18	22	5,1	8	0,5	368	2x10E-5	6,5	30
19		5,1			372			
20		5,2			374			
5		5,5			390			

Adhesive niobium nitride coatings with typical grey-yellowish color were obtained (Fig.5.4).
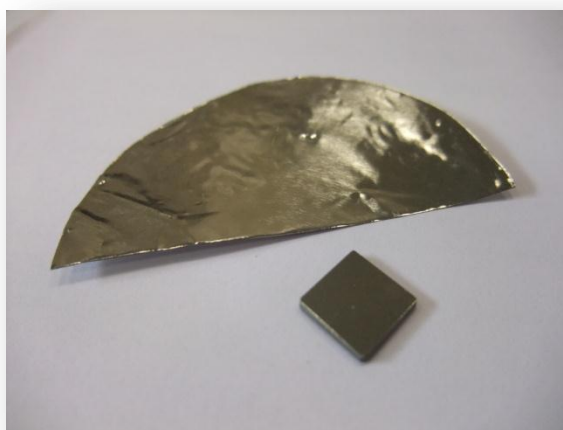
Fig.5. 4 Niobium nitride film obtained at 22 ˚C substrate temperature

For all coatings the thicknesses were measured. Cubic lattice parameters were calculated and plotted in comparison with standard value (Fig.5.5). Values of calculated average grain sizes, lattice parameters and thicknesses were collected in *Table 5.4*.

Table 5. 4 Parameters of NbN films obtained at room temperature temperature

Sample, №	Thickness, nm	Deposition rate, nm/sec	Cubic lattice parameter, Å	Average grain size, Å
NbN standard	-	-	4,4090	-
1	1300	0,7222	4,3823	245
13	1200	0,6667	4,3719	285
17	1300	0,7222	4,3797	220
4	1500	0,8333	4,3847	270
18	1300	0,7222	4,3854	330
19	1200	0,6667	4,3864	325
20	1200	0,6667	4,3816	290
5	1150	0,6389	4,3846	270
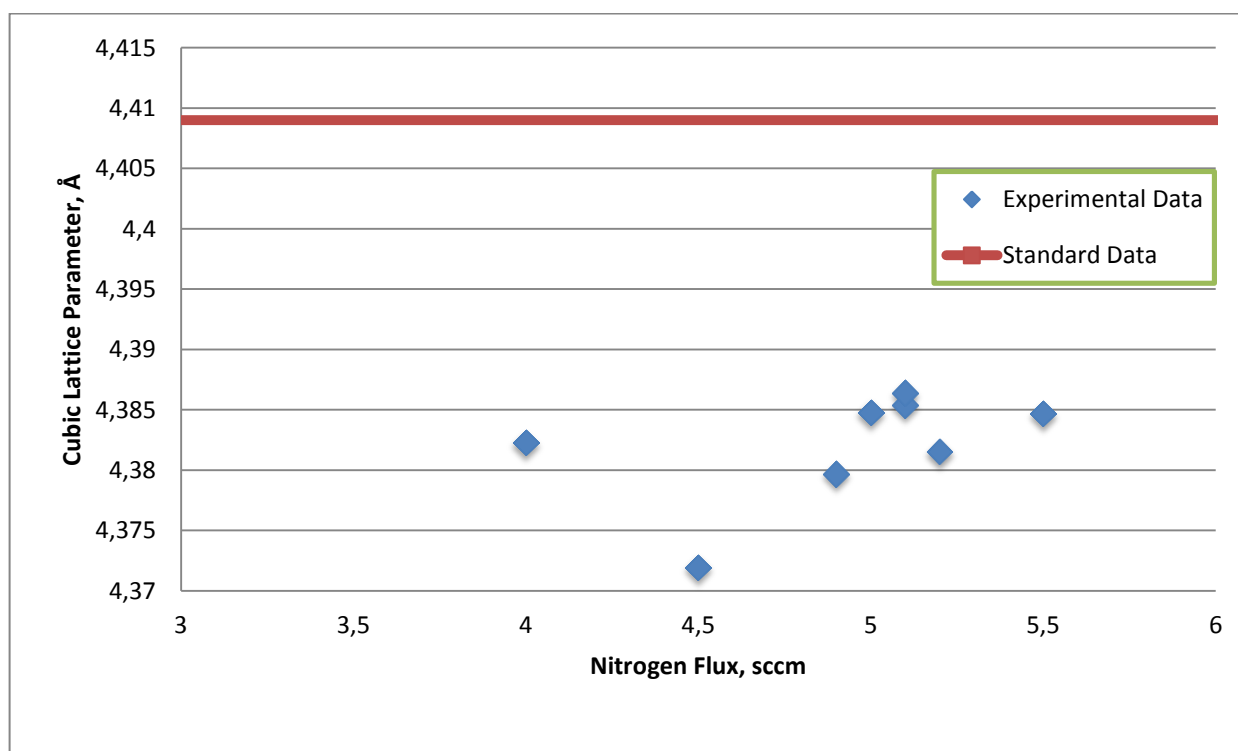
Fig.5. 5 Cubic lattice parameters for NbN coatings obtained at room temperature

Samples 18, 19, obtained at N_2 flux 5,1 sccm, had lattice parameters closest to the standard value. So this is the best conditions to obtain stochiometric NbN coatings at room temperature.

At fixed gas flux (Ar 8 sccm, N_2 5,1 sccm), sputtering at different temperatures was performed (*Table 5.5*). Corresponding coating parameters are presented in *Table 5.6*.

Table 5. 5 Deposition parameters for sputtering deposition of NbN films

Sam-ple, №	Substrate temperature, ˚C	Nitrogen flux, sccm	Argon flux, sccm	DC current, A	DC tension, V	Base pressure, mbar	Target-substrate distance, cm	Deposition time, min
21	Floating(90˚C)	5,1	8	0,5	374	2x10E-5	12,2	30
22	200				378		12,2	
24	Floating, plasma cleaned				390		7,5	
25	500				390		12,2	

Table 5. 6 Parameters of NbN films obtained at floating temperature and 200 ˚C

Sample, №	Thickness, nm	Deposition rate, nm/sec	Cubic lattice parameter, Å	Average grain size, Å
NbN standard	-	-	4,4090	-
21	350	0,1944	4,3656	220
22	400	0,2222	4,3624	330
24	800	0,4444	4,3774	170
25	200	0,1111	4,3448	300

Changing substrate temperature, we change NbN film composition. On the base of previous experience, we believed that rising substrate temperature, we could obtain coatings with better lattice parameter. But after experiments we found that rising substrate temperature up to 500 ˚C we decresed the value of cubic lattice parameter for NbN coatings (Fig. 5.6). Probably at high temperatures, weak Nb---N bonds dissociate rather than form stable compounds and we get understochiometric composition of the coating. To improve the value of cubic lattice parameter at high temperatures, we should increase nitrogen flux.

Also it should be noticed that calculated average grain sizes (Fig.5.7) differ while changing substrate temperature during deposition as well. At higher temperature we increased crystallinity of our films.
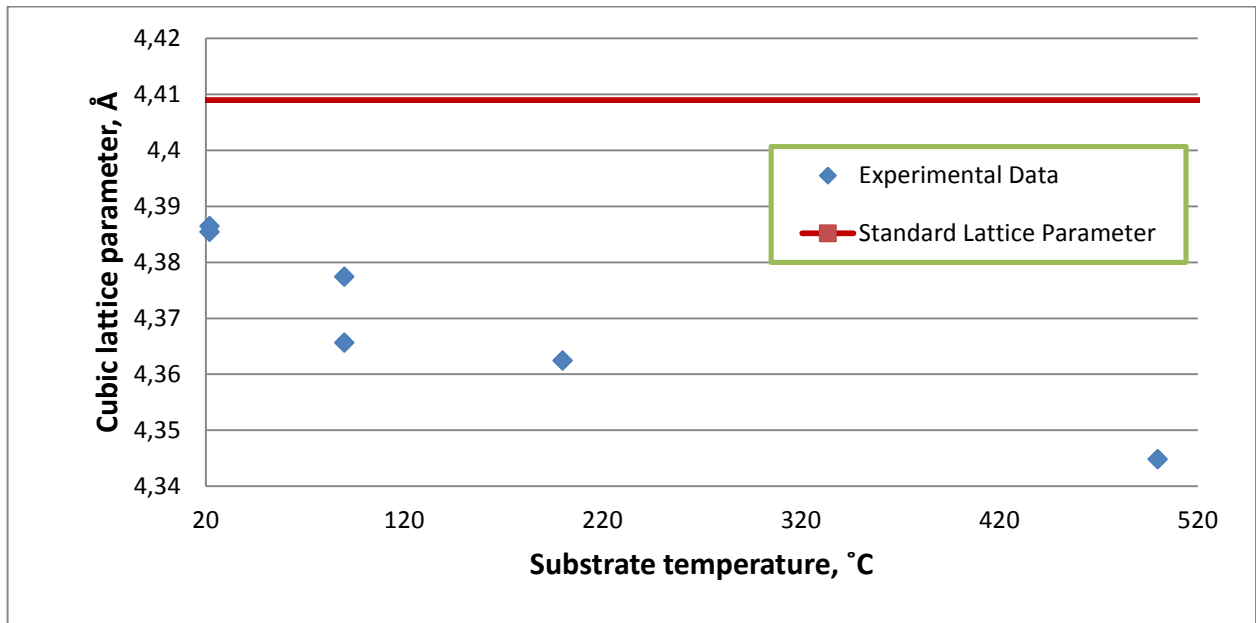
Fig.5. 6 Cubic lattice parameters for NbN coating obtained at different substrate temperatures (N₂ flux 5,1 sccm)
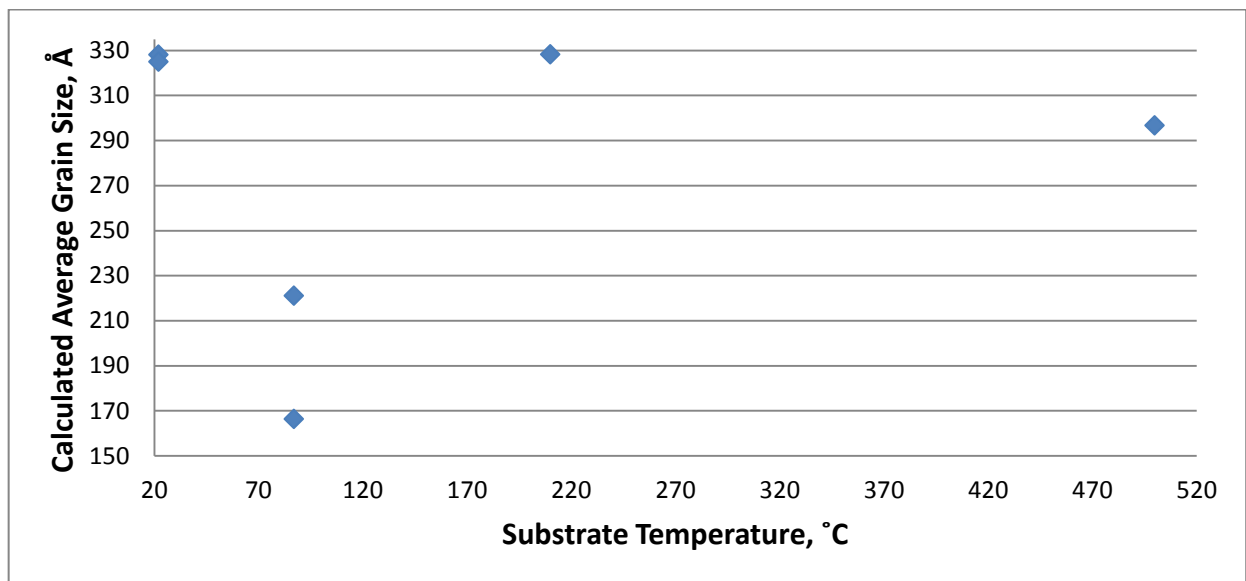
Fig.5. 7 Calculated average grain size for NbN coating obtained at different substrate temperatures (N₂ flux 5,1 sccm)

Coatings obtained at room temperature, had the lattice parameter closest to standart value. We also can notice that increasing substrate temperature, we increase crystallinity of the coating, but still anomalous stays the similatity of this parameter for films deposited at room temperature substrate and at 200 ˚C.

At the Fig. 5.8 the morphology of niobium nitride coatings is shown. We can see that after deposition at room temperature the cracks on the surface were formed. The tensile stress could

occur due to different thermal expansion coefficients for aluminum substrate and niobium nitride coating while temperature gradient across the sample.
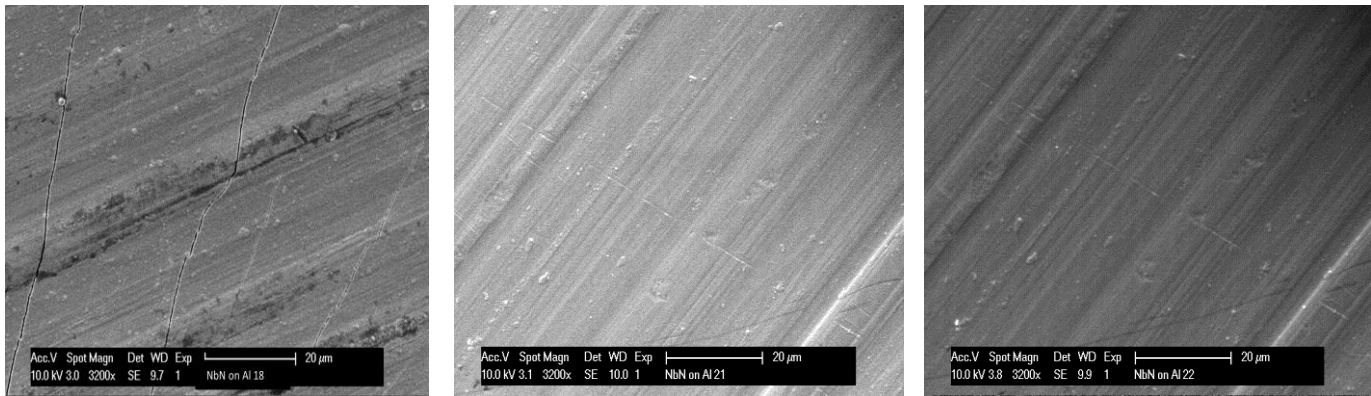
Fig.5. 8 SEM micrographs of NbN coatings obtatined at different substrate temperatures: a) 22 ˚C (NbN 18), b) floating temperature (NbN 21), c) 200 ˚C (NbN 22)

XRD spectrums of NbN coatings were obtained. All of them have characteristic peaks which correspond to the standard data. As an example, NbN 24 coating, obtained at floating temperature and substrate plasma cleaning before deposition is shown below:
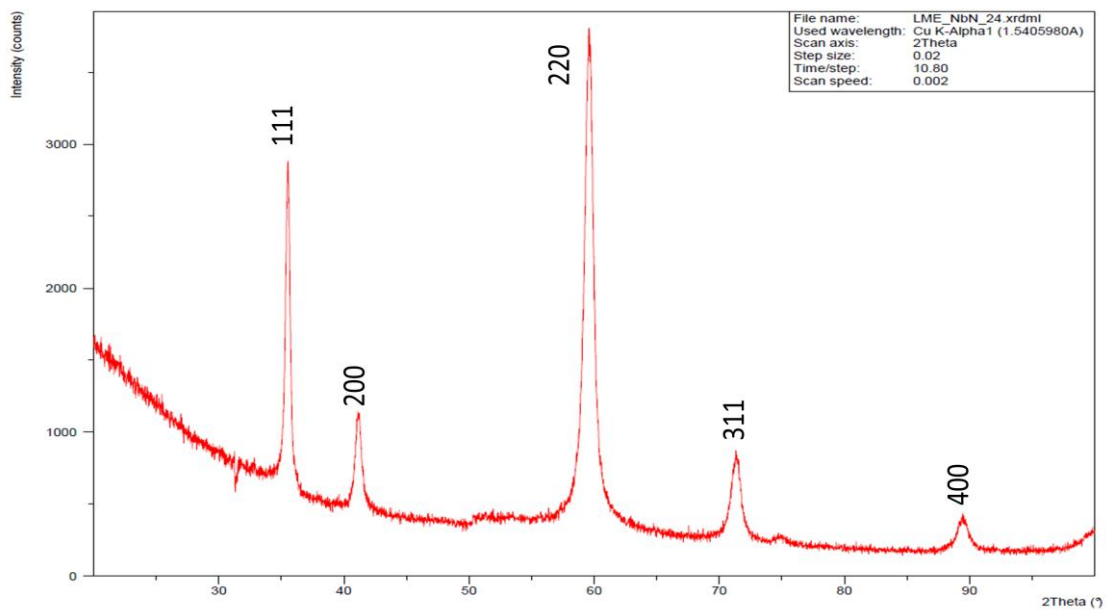
Peak list

No.	h	k	l	d [A]	2Theta[deg]	I [%]
1	1	1	1	2.53688	35.353	100.0
2	2	0	0	2.19700	41.050	80.6
3	2	2	0	1.55351	59.451	43.6
4	3	1	1	1.32484	71.102	29.6
5	2	2	2	1.26844	74.786	12.6
6	4	0	0	1.09850	89.051	5.2
7	3	3	1	1.00805	99.663	10.6
8	4	2	0	0.98253	103.256	14.7
9	4	2	2	0.89692	118.370	11.9
10	5	1	1	0.84563	131.266	9.7

Fig.5. 9 XRD spectrum of NbN (№24) coating obtained at floating temperature

5.2.2 Test with liquid gallium

Obtained niobium nitride coatings were tested against liquid gallium corrosion at static conditions (Chapter 2.5).

We can see that different deposition parameters affect the coating structure and thus interaction between coating surface and gallium.

In fact, already at room temperature test, liquid gallium corrodes coatings sputtered at room substrate temperature and not optimal nitrogen flux (understochionetric composition).

At 50˚C test, Ga immediately wets NbN coatings sputtered at room temperature (N_2 flux 5.1 sccm) and leaves only small traces on coatings with higher temperature substrate (200 ˚C, floating) during deposition. The same behavior of last mentioned coatings was observed after interaction with Ga at 100 and 200 ˚C (Fig. 5.10).
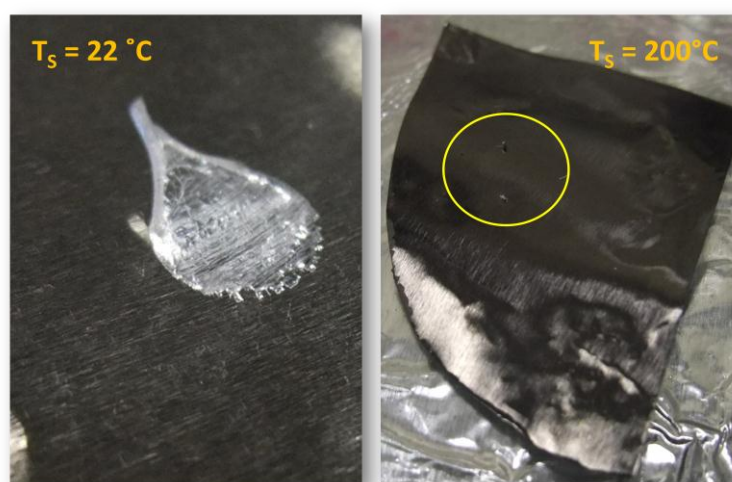
Fig.5. 10 NbN coatings after interaction with liquid gallium

As we see from SEM micrograph (Fig.5.8), the coatings №18, obtained at 22 ˚C had cracks, which probably were the reason of higher wettability of Ga on this surface.

Though no embrittlement or corrosion was observed on discussed above samples even after 6h heating at 200 ˚C with gallium drop.

We can conclude that for obtaining niobium nitride coatings, resistant to liquid gallium penetration, we must take into account following deposition parameters: stochiometric film composition, substrate plasma cleaning and substrate temperature while deposition. Thus, NbN coatings which were obtained at higher substrate temperatures (200, 500 ˚C) resist better.

5.3 CONCLUSIONS

Surfaces of niobium nitride coatings, obtained within the bounds of this project, become wet after interaction with liquid gallium, but it does not cause embrittlement even after a long heating at 200 ˚C. All of them were obtained at 8 sccm Ar and 5,1 sccm N_2 flux, current 0,5 A, base pressure 10E-5 mbar.

Depositing such coatings, we should firstly perform plasma cleaning of the substrate and to start sputtering immediately after that. Stochiometric composition as well as deposition substrate temperature play an important role. Thus, NbN coating obtained at floating temperature or with heating (500 ˚C) have lower wettability by gallium than coatings obtained at room temperature. According to XRD spectrums, they had higher level of crystallinity, but cubic lattice parameter was degradating while rising substrate temperature.

If to compare NbN to Nb coatings, we could say, that niobium nitride obtained at high substrate temperature (>200 ˚C) has lower wettability by gallium than Nb coating, thus, they are supposed to be better barriers against liquid metal embrittlement.

CHAPTER 6. CERIUM OXIDE THIN FILMS

6.1 THEORETICAL BACKGROUND

6.1.1 Structure

Ceria is an oxide of rare earth metal cerium Ce. It is a pale yellow-white powder with the chemical formula CeO_2(Fig.6.1). Cerium also forms cerium(III) oxide, Ce_2O_3, but CeO_2 is the most stable phase at room temperature and under atmospheric conditions. Ceria has a cubic (fluorite structure). In the most stable fluorite phase of ceria, it exhibits several defects depending on partial pressure of oxygen. The primary defects of concern are oxygen vacancies. In the case of oxygen defects, the increased diffusion rate of oxygen in the lattice causes increased catalytic activity as well as an increase in ionic conductivity, making ceria interesting as a fuel cell electrolyte in solid-oxide fuel cells.
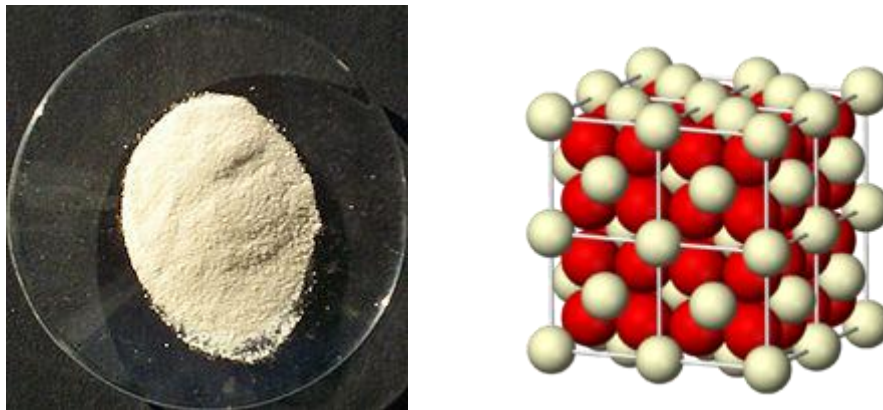
Fig.6. 1 Ceria powder and its structure

6.1.2 Obtaining

Cerium(IV) oxide is formed by the calcination of cerium oxalate or cerium hydroxide[90].

Cerium dioxide particles can be also synthesized by using the room temperature reaction of cerium nitrate and hexamethylenetetramine[91].

6.1.3 Properties

Cerium oxide's density is 7,215 g/cm^3. It has high melting and boiling points (2400 and 3500 ˚C correspondingly). Powdered ceria is slightly hygroscopic and will also absorb a small amount of carbondioxide from the atmosphere[92].

The experimental [93], [94] thermal expansion coefficient of CeO_2 and that calculated are shown in Fig. 6.2[95].
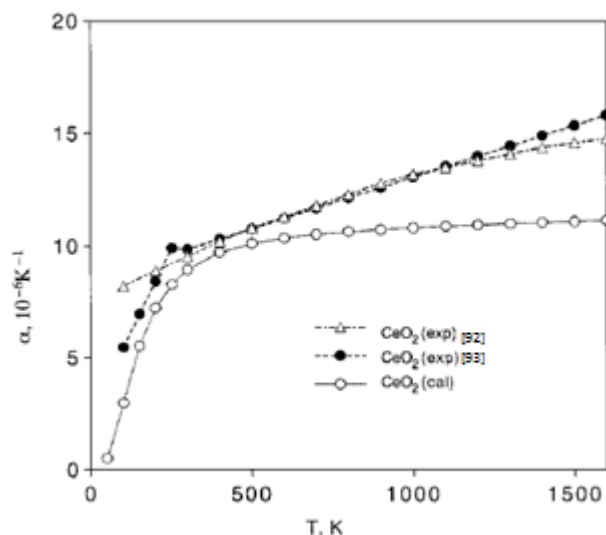
Fig.6. 2 Thermal expansion coefficients of cerium dioxide

Cerium oxide is known for its high chemical and thermal stability[96], which makes it an excellent component for three way catalysts (TWCs) that can convert simultaneously CO to CO_2, hydrocarbons to CO_2 and H_2O (i.e. oxidation reactions) and also NO_x to N_2 (i.e. reduction reactions)[97].

6.1.4 Application

Cerium(IV) oxide is used in ceramics, to sensitize photosensitive glass, as a catalyst and as a catalyst support, to polish glass and stones, in lapidary as an alternative to "jeweller's rouge". It is also known as "optician's rouge"[98].

It is also used in the walls of self-cleaning ovens as a hydrocarbon catalyst during the high-temperature cleaning process.

While it is transparent for visible light, it absorbs ultraviolet radiation strongly, so it is a prospective replacement of zinc oxide and titanium dioxide in sunscreens, as it has lower photocatalytic activity.

Cerium oxide particles are of interest because of possible applications in catalysis [99] and fuel cell technologies[100]. Oxygen defects in these particles make them complex to understand, yet useful.

6.2 EXPERIMENTAL PART

6.2.1 Obtaining and analyses of CeO₂ coatings

Transparent CeO_2 films (Fig. 6.3) were obtained by reactive DC magnetron sputtering in vacuum chamber with the base pressure 2x10E-5 mbar (chapter 2.3). Cerium target was bombarded with argon. Oxygen was used as a reactive gas to form cerium oxide. Deposition parameters are described in *Table 6.1*.
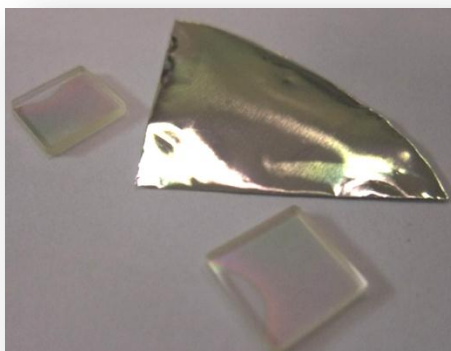
Fig.6. 3 Ceria film (№21) on aluminum and quartz substrates

Ceria films with stochiometric composition were transparent and had yellowish color with typical interference rings (Fig.6.3) which appeared probably due to different coating thickness. Different thickness could be explained by magnetron configuration and fixed not rotating sample holder. Even though, cerium oxide coatings were adhesive to the substrate and didn't change with the course of time.

If the ratio $Ar:O_2$ is not right (causing understochiometric films composition), ceria films have yellow metallic color and it turns into blue with time due to further oxidation process (Fig. 6.4).
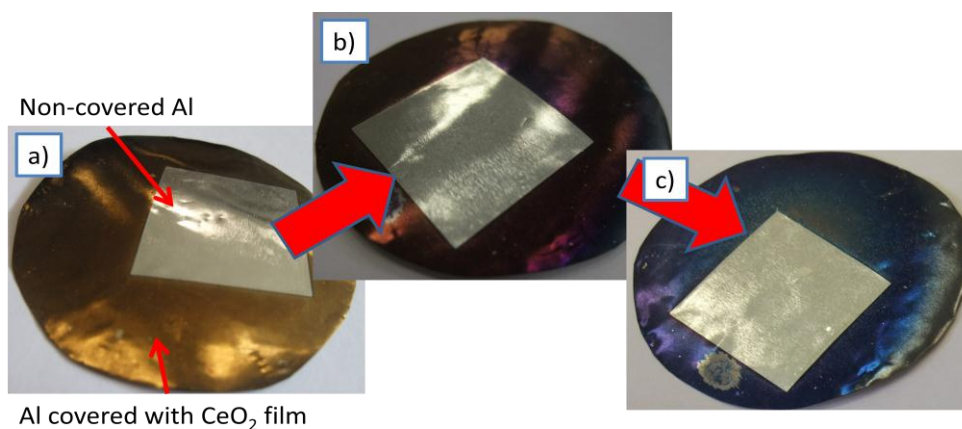
Fig.6. 4 Understochiometric CeO₂ films: a) after deposition, b) in 2 days and c) in 2 weeks after deposition

Table 6. 1 Deposition parameters to obtain CeO$_2$ coatings

Sample, №	Substrate temperature, ˚C	Oxygen flux, sccm	Argon flux, sccm	DC current, A	DC tension, V	Base pressure, mbar	Plasma cleaning of substrate	Bias tension, V	Target-substrate distance, cm	Deposition time, min
15	22	4	8		240		-		6,5	120
19	floating				300		+		7,5	120
20	floating	1. 0 2. 4	1. 8 2. 8		1. 280 2. 300		+			130
21	250 (end temp., floating)				300			-		120
22	350				300				12,0	120
23	350			0,5	300	2x10E-5	-			120
24	500				300					240
25	floating	4	8		300			50		30
26	floating				300				7,5	30
27	floating				300		+	-		30
28	500				275		-		12,0	30
29	floating				260		+	50	7,5	60

Ceria films were obtained at different substrate temperatures – floating, 22, 250, 350 and 500 ˚C. The optimum gas flux, which consists of 8 sccm Ar and 4 sccm O_2, was found in a previous work[101] and used in the current project.

On the sample holder, which was possible to connect to the voltage supply, the obtaining of cerium oxide coating was held on plasma discharge cleaned substrate and at floating substrate temperature.

The influence of bias potential on coating properties was also studied. It is well known that bias potential increases the ion flux to the substrate; thereby it takes part in film hardening and densification. But in addition another process can possibly occur - sputtering of growing film. In our case it is probably not desired, since it reduces the effective growth rate or may deteriorate the quality of the material due to formation of defects at the surface or in the bulk.

On sample №20, Ce metal was deposited as an interlayer between substrate and CeO_2 coating. Before deposition the substrate was cleaned by plasma discharge.

After deposition, all coatings were analyzed and their parameters were collected in *Table 6.2*. If the substrate temperature increases, the rate of thermal desorption from the weakly-adsorbed state increases leading to decreasing of effective sputtering rate (*Table 6.2*, Fig.6.5). Along this process, we observe changing of lattice parameter (Fig.6.6).

Table 6. 2 Parameters of obtained CeO_2 coatings

Sample, №	Substrate temperature, ˚C	Thickness, nm	Deposition rate, nm/sec	Cubic lattice parameter, Å	Average grain Size, Å
CeO_2 stand.	-	-	-	5,4110	-
15	22	1500	0,2083	5,4419	120
19	floating	1600	0,2222	-	-
20	floating	1800	0,2307	5,4613	210
21	250 (floating)	400	0,0556	5,4711	150
22	350	300	0,0417	5,4532	335
23	350	270	0,0375	5,4633	350
24	500	650	0,0451	5,4484	390
25	floating	300	0,1667	5,4600	120
26	floating	220	0,1222	5,4609	130
27	floating	200	0,1111	5,4615	130
28	500	60	0,0322	5,4522	325
29	floating	600	0,1684	5,4696	120
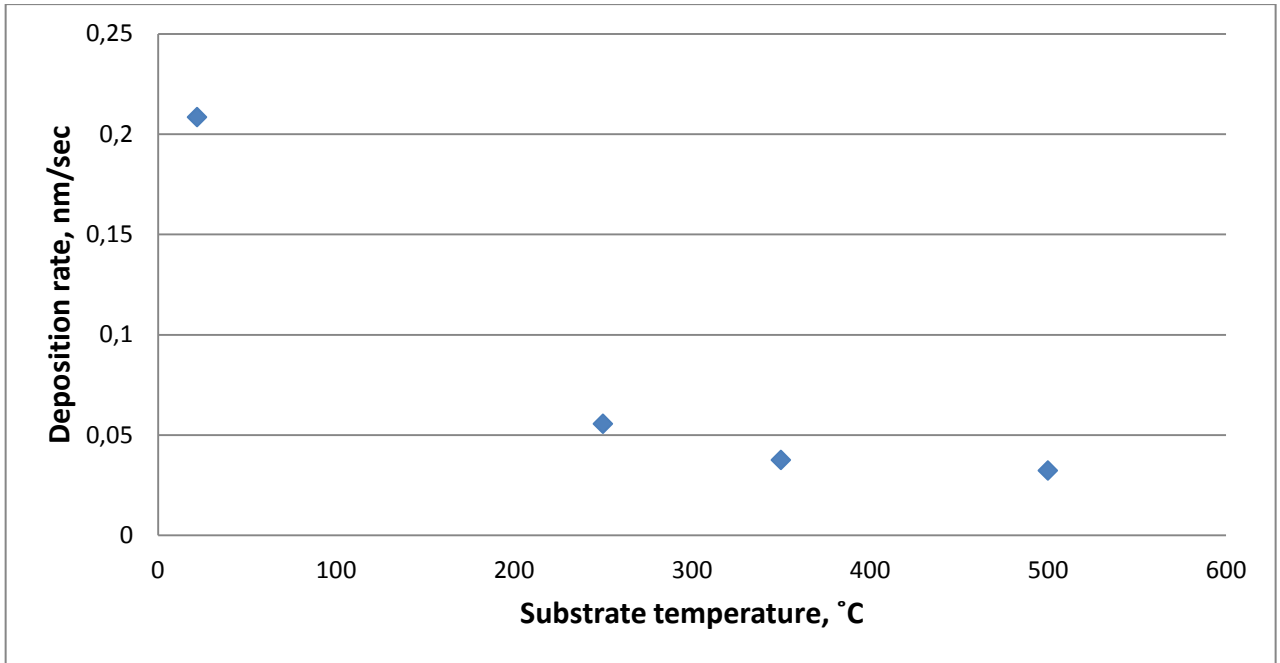
Fig.6. 5 Deposition rate of ceria coatings obtained at different substrate temperatures
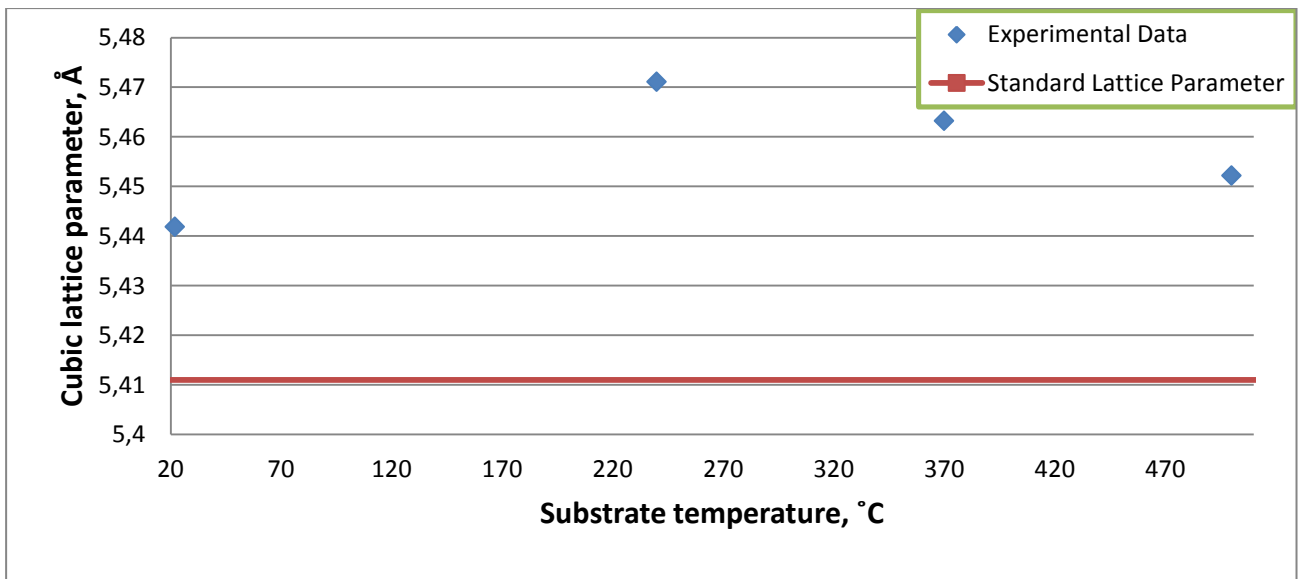
Fig.6. 6 Cubic lattice parameter for ceria coatings obtained at different substrate temperature

We can see that lattice parameter for coating obtained at floating (≈200 ˚C) temperature is much higher that at room temperature. And further, with rising substrate temperatre, the slope for lattice parameter goes down. Interestingly, those coatings with less ordered structure showed better resistance against liquid gallium (floating $T_{substrate}$).

The morphology of obtained coatings was studied by SEM microscopy (Fig.6.7).
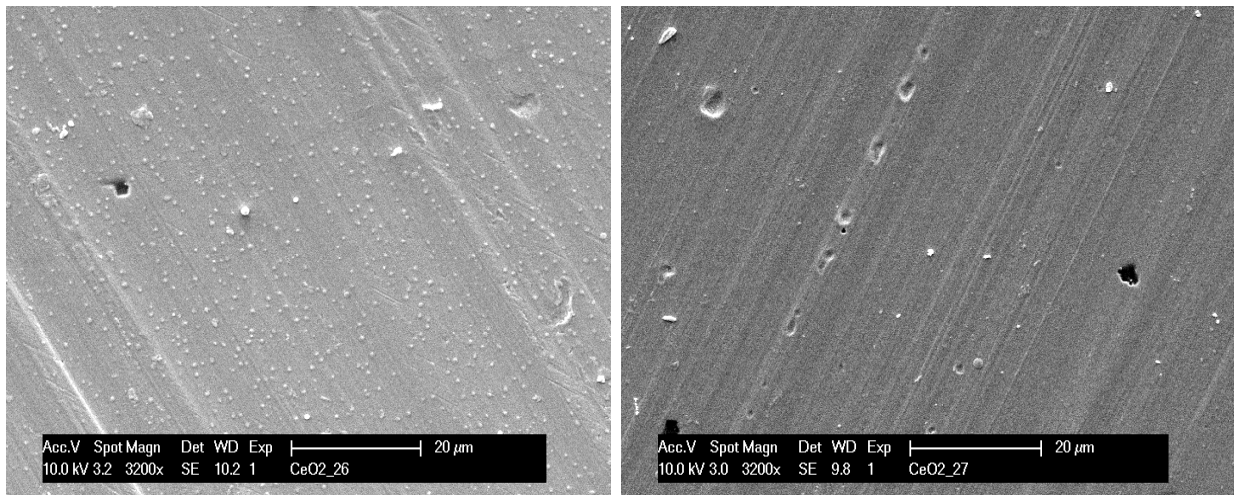
<div align="center">a)</div>
<div align="center">b)</div>

Fig.6. 7 SEM micrographs of CeO₂ films obtained at floating temperature: not plasma cleaned , b) plasma cleaned substrate

Coatings, which were deposited after plasma discharge cleaning of the substrate, have more flat and smooth surface, without any inclusions and regular imperfections.

We observed that with rising substrate temperature, the crystallinity of coatings increased, which was calculated by Debye-Schrerrer formula (Fig.6.8). We also can observe this from the XRD spectrums (Fig. 6.9) – the characteristic peak (111) shape was becoming sharper and more well-defined with rising substrate temperature. It is interesting that average grain size of ceria films obtained at 22 ˚C is almost equal to those obtained at floating temperature applying bias potential. The full XRD spectrum of one of CeO₂ coating is presented on Fig. 6.10. All peaks correspond to standard XRD peaks for CeO₂.
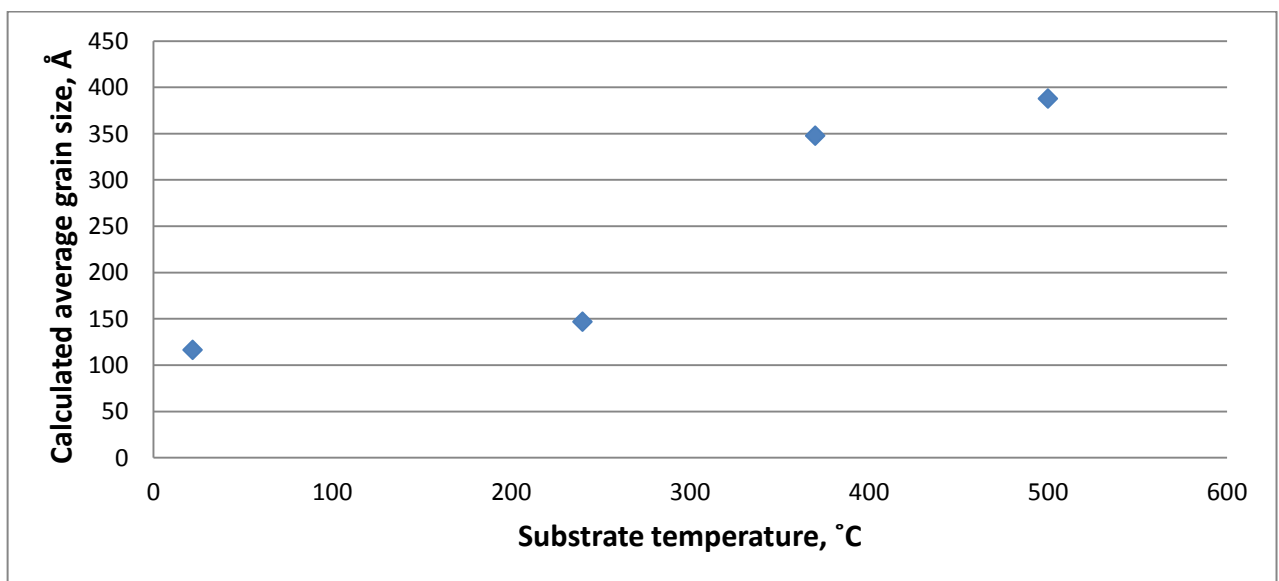
Fig.6. 8 Calculated average grain size for ceria coatings obtained at different substrate temperature
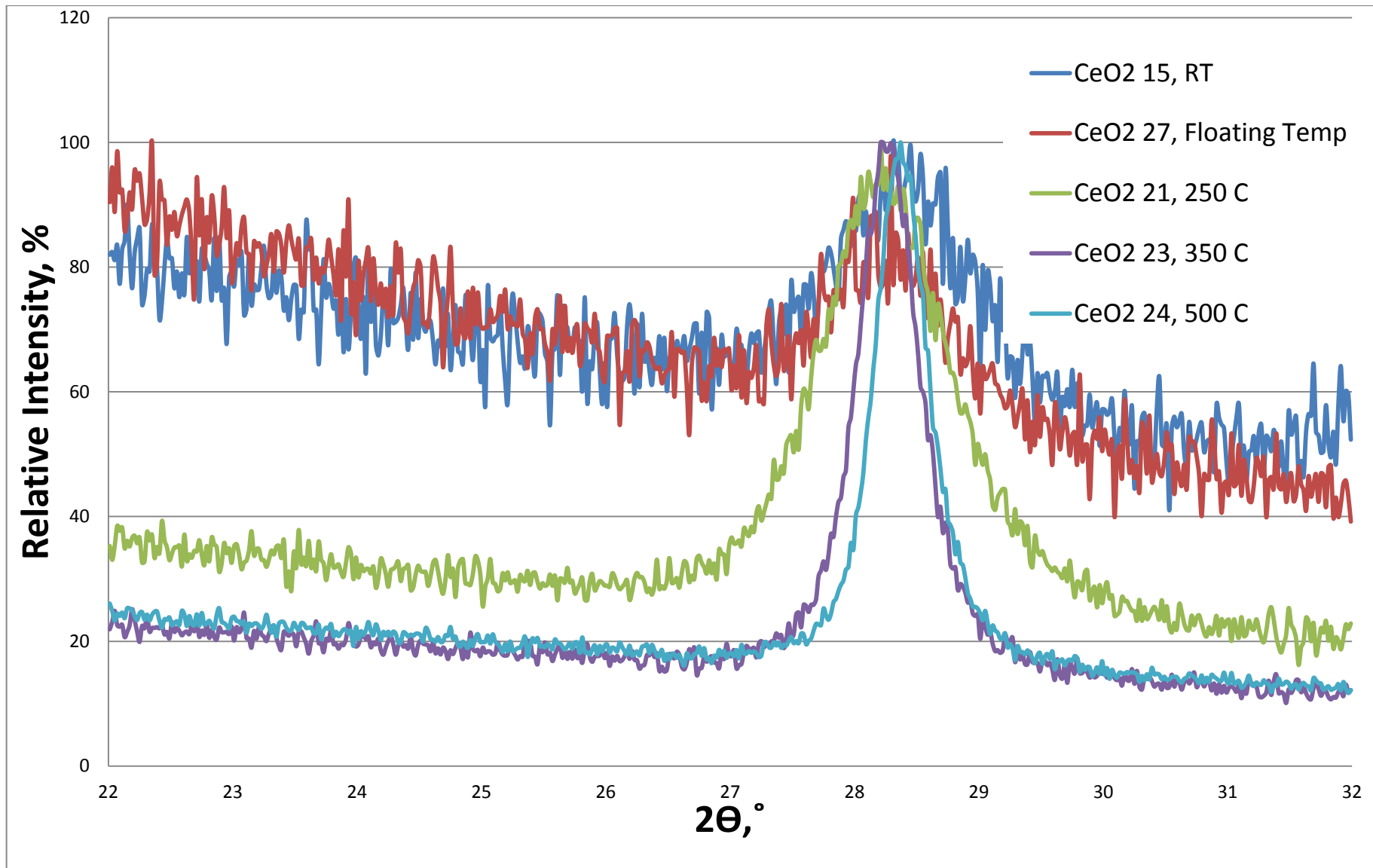
Fig. 6.9 Comparison of XRD characteristic peaks of ceria coatings obtained at different substrate temperature
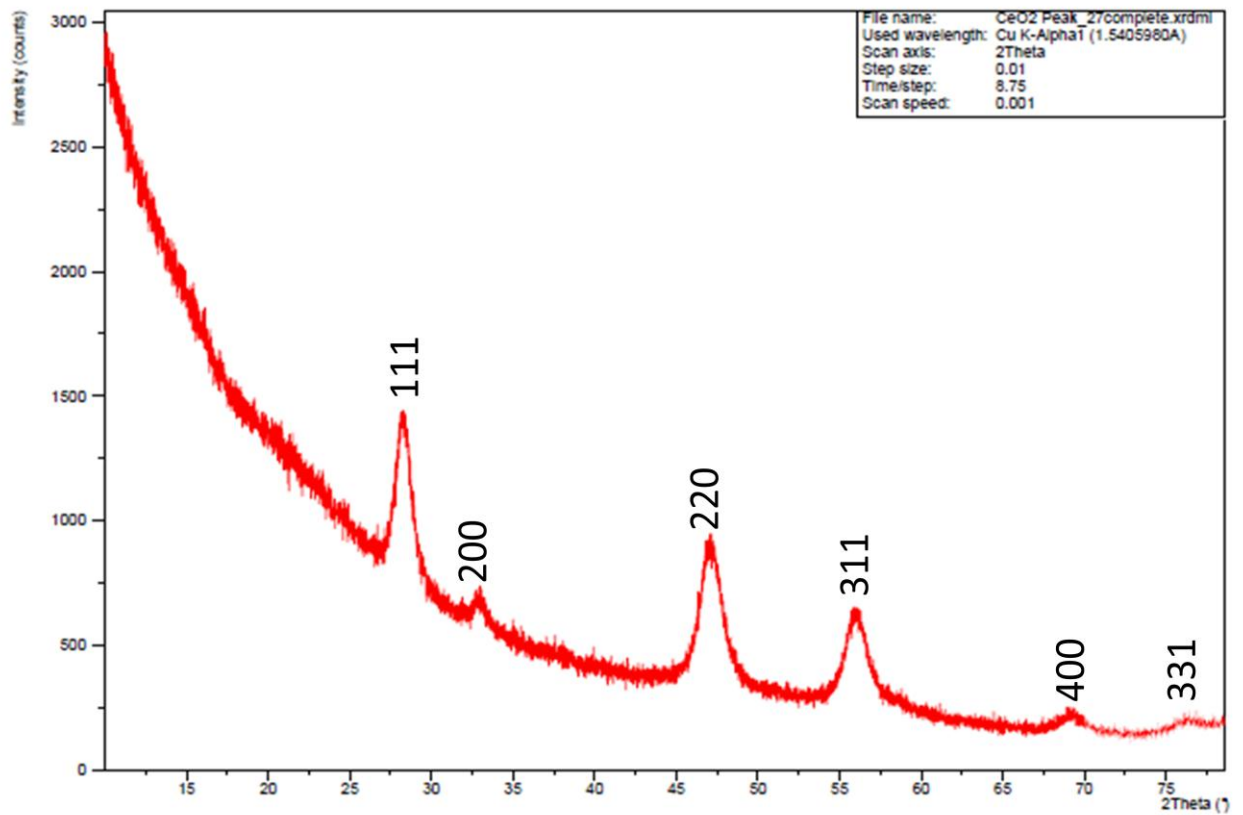
Peak list

No.	h	k	l	d [A]	2Theta[deg]	I [%]
1	1	1	1	3.19044	27.943	100.0
2	2	0	0	2.76300	32.376	29.9
3	2	2	0	1.95374	46.441	45.1
4	3	1	1	1.66615	55.074	34.2
5	2	2	2	1.59522	57.747	6.5
6	4	0	0	1.38150	67.778	5.4
7	3	3	1	1.26775	74.834	11.0
8	4	2	0	1.23565	77.129	7.1
9	4	2	2	1.12799	86.141	8.9
10	5	1	1	1.06348	92.825	7.2
11	4	4	0	0.97687	104.099	2.6
12	5	3	1	0.93406	111.111	7.1
13	4	4	2	0.92100	113.518	3.3
14	6	2	0	0.87374	123.676	4.0
15	5	3	3	0.84271	132.150	3.0
16	6	2	2	0.83308	135.230	2.3
17	4	4	4	0.79761	149.927	1.2

Fig.6. 9 Full XRD spectrum of CeO₂ (№27) film deposited at floating substrate temperature

6.2.2 Test with liquid gallium

CeO$_2$ films were tested against liquid gallium embrittlement. The test was performed as described in Chapter 2.5. Obtained at different deposition parameters, hence with different structure and properties, ceria coatings interacted with gallium in different ways.

Coatings, obtained at room temperature, at first were wet by liquid metal at 22 ˚C interaction temperature, and then corroded. The CeO$_2$ film shrinked and cracked, so Ga penetrated through it into the bulk (Fig.6.11).

Fig.6. 10 Penetration of Ga into CeO$_2$ coating obtained at room temperature

Coatings, sputtered at 350 and 500 ˚C substrate temperature, corroded almost immediately after interaction with gallium even at 22 ˚C (Fig.6.12a). Should be noticed that for assembling of Al to the sample holder for high temperature experiments (>200 ˚C), we should not use silver glue, it is better to fix samples mechanically. Indeed, an interface reaction between Ag and Al was observed after deposition and aluminum changed its shape (shrinked).

Bias potential didn't improve properties of ceria films in a context of barrier protection. Ga leaves its traces on the surface (Fig.12b).
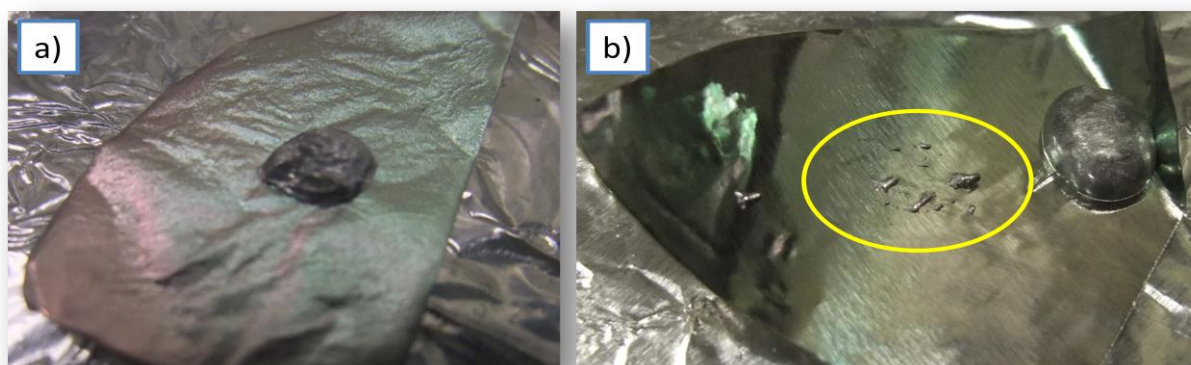
Fig.6. 11 Interaction between liquid gallium and ceria coatings: a) coating obtained at 500 ˚C substrate temperature, b) bias 50 V

Coatings №19 and 20, obtained at floating temperature with plasma cleaning of the substrate before deposition, were not wet by gallium. In case of sample 20, Ce metal was used as an interlayer between aluminum and ceria. The gallium drop was removed from the surface after 9h heating at 200 ˚C; after that no visual traces of gallium were observed. Coatings, obtained at floating temperature, but deposited on plasma discharge cleaned substrate, behaved the same way (Fig.6.12).
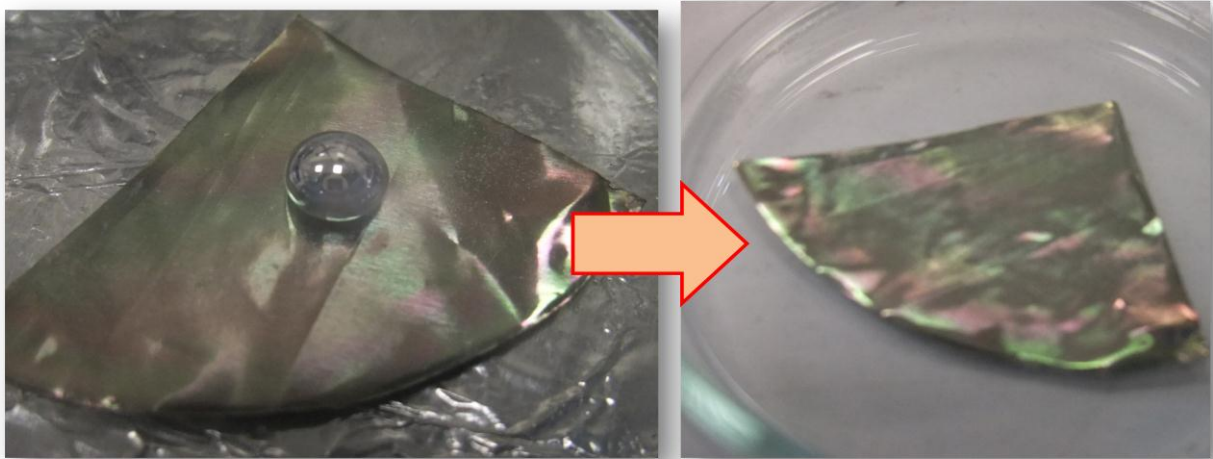
Fig.6. 12 Interaction of liquid gallium and ceria coating (№27)

6.3 CONCLUSIONS

Adhesive transparent ceria films were obtained by DC magnetron reactive sputtering. Different deposition parameters were performed and properties of obtained films were analyzed. It was found that coatings, resistant to penetration of liquid gallium, must be firstly deposited on plasma cleaned substrate and deposition must be performed at floating substrate temperature. These coatings didn't become wet by Ga even after 9h of interaction at 200 ˚C.

High substrate temperature raises crystallinity of the coating; hence it is easier for gallium to penetrate through grain boundaries and to cause embrittlement.

But we can not control floating temperature, especially in industrial scale. It will depend on many parameters; the main of them is magnetron size.

CONCLUSIONS AND SUGGESTIONS FOR FUTURE WORK

Within the frames of this project, protective coatings against liquid gallium embrittlement have been succesfully obtained by magnetron sputtering.

It was found that varying the gas flux (gas partial pressure) and substrate temperature we change the structure of the growing film. According XRD spectrums and calculated average grain size by Debye-Schrerrer formula, it was shown that rising substrate temperature we increase crystallinity and level of order of deposited films. Right reactive gas flux leads to stochiometric composition of the coating. Both parameters are of first importance for obtaining films which are resistant against gallium corrosion.

After carrying out the static test – interaction of obtained films with liquid gallium at atmospheric conditions, niobium and niobium nitride coating did not corrode and did not become brittle in presence of liquid gallium. Gallium wets their surfaces but does not penetrate further into the bulk due to probably formation of gallium oxides which work as blockers. To understand this process, more advanced test under inert atmosphere should be carried out. After that coatings should be examined on the surface and across the section by, for example, SEM microscopy. If gallium oxides work as barriers for further penetration of Ga into the material, then these oxides could also be proposed as a solution of current problem.

It was found, that gallium is not soluble in cerium oxide coatings obtained at floating temperature after preliminary substrate cleaning by plasma discharge. They had much higher lattice parameter, than other samples. These coatings resist even at 200 ˚C continuous heating. It will allow using gallium and its alloys as safe and efficient coolants for nuclear reactor cores and cyclotron targets.

The table with main parameters of coatings, resistant to LME caused by gallium are displayed in the following table:

Table.7. 1 Parameters of sputtered coatings and interaction with Ga

Film	$T_{depos.}$, ˚C	Ar flux, sccm	N_2 flux, sccm	O_2 flux, sccm	I_{DC}, A	Thickness, nm	Interraction with Ga
Nb	22		0	0		1000	wet
NbN	500	8	5,1	0	0,5	200	traces of Ga
CeO$_2$	floating		0	4,0		200	resistant

Diamond-like carbon coatings were not tested against liquid gallium penetration. The sputtering system should be modified and run over again in order to get hard adhesive films. The advantage of DLC in comparison with Nb, NbN and CeO_2, is high thermal conductivity which is one of the most important factors for cooling systems as well as corrosion resistance. Thus, development of cooling systems covered by DLC films continues to be very promising and interesting direction.

It should be mentioned, that after successful static test of obtained coatings with liquid gallium, dynamic test is required. It is important to observe the behavior of protective films under rapid coolant flow which will simulate the real conditions.

LIST OF TABLES

LIST OF FIGURES

REFERENCES

[1] "DOE Fundamentals Handbook: Nuclear Physics and Reactor Theory", *US Department of Energy*, rchived from the original on 23 April 2008, retrieved 24 September 2008

[2] "Reactor Protection & Engineered Safety Feature Systems", *The Nuclear Tourist,* retrieved 25 September 2008

[3] "Generation IV Nuclear Reactors", *World Nuclear Association*, 2010

[4] Sang Hun Shin, Jong Jin Kim, Ju Ang Jung*, Journal of Nuclear Materials*, 92–102, 2012

[5] J. Huntington, *Inst. Metals* 11, 108, 1914

[6] D.G. Kolman and R. Chavarria, *Journal of Testing and Evaluation* 30, 452, 2002

[7] D.G. Kolman, *ASM Handbook* 13A, , ASM International, Materials Park, OH, 393-397, 2003

[8] M. H. Kamdar, *Academic Press* 25, 361, 1983

[9] B. Joseph, M. Picat, and F. Barbier, Eur. *Phys. J. AP* 5 , 19, 1999

[10] Liquid metal assisted cracking of galvanized steel work, Topic Paper, SC / T / 04 / 02, *Standing Committee on Structural Safety*, London, U. K. June 2004, website: www.scoss.org.uk

[11] D.G. Kolman, *ASM Handbook* 13A, ASM International, Materials Park, OH, 381-392, 2003

[12] W. M. Robertson, *Trans. Met. Soc. AIME*, 236, 1478, 1996

[13] E. E. Glickman and Y. V. Goryunov, *Sov. Mater. Sci*., 355, 1978

[14] N. S. Stoloff and T. L. Johnston, *Acta Met*., 11, 251, 1963

[15] A. R. C. Westwood and M. H. Kamdar, *Phil. Mag*., 8, 787, 1963

[16] P. Gordon and H. H. Ann, *Met. Tr*ans., A 13, 457, 1982

[17] S. P. Lynch, *Acta Met*., 36, 2639, 1988

[18] V. V. Popovich, and I. G. Dmukhovskaya, *Sov. Mater. Sci*., 535, 1987

[19] Ina K and Koizumi, *Mater. Sci. Eng*. A 387-389, 390, 2004

[20] Roques-Carmes C, Aucouturier, M. and Lacombe P , *Metal Sci. J.* 7 128, 1973

[21] Hugo R C and Hoagland R G, *Scripta Mater*. 38 523, 1998

[22] Hugo R C and Hoagland R G, *Acta Mater*. 48 1949, 2000

[23] Ludwig W and Bellet D, *Mater. Sci. Eng*. A 281 198, 2000

[24] Pereiro-L´opez E, Ludwig W, Bellet D, Cloetens P and Lemaignan, *Phys. Rev. Lett*. 95 215501, 2005

[25] Hugo R C and Hoagland R G, Scripta Mater. 41 1341, 1999

[26] J.A. Thornton, A.S. Penfold, *Thin Film Processes*, *Academic, New York*, 1987

[27] K. Wasa, S. Hayakawa, *Rev. Sci. Instrum*. 40, 693 1969

[28] F.A. Green, B.N. Chapman, *Appl. Phys. Lett*. 27, 189 1975

[29] W.D. Gill, E. Kay, *Rev. Sci. Instrum*. 36, 277, 1965

[30] J.A. Thornton*, J. Vac. Sci. Technol*. 15 (2), 171-177, 1978

[31] R.K. Waits, J. *Vac. Sci. Technol*. 15, 179, 1978

[32] D.B. Fraser, *J. Vac. Sci. Technol*. 15, 178, 1978

[33] J.A. Thornton, V.L. Hedgcoth, *J. Vac. Sci. Technol*. 12, 93, 1975

[34] D.A. Glocker, S.I. Shah, *Handbook of Thin Film Precess Technology* (Institute of Physics, Philadelphia, 1995

[35] M.J. Goeckner, T.K. Bennett, S.A. Cohen, *Appl. Phys. Lett*. 71, 980, 1997

[36] M.Marinov, *Thin Solid Films* 46, 267, 1977

[37] J.E. Greene, *CRC Crit. Rew. Solid State Mater. Sci*. 11, 47, 983

[38] V.J. Nizhenko, L.I. Sklyarenko, V.N. Eremenko, *Ukr. Khim. Zh*. 6 , 559, 1965

[39] A.G.M. Nalgiev, Kh. Ibragimov, *Zh. Fiz. KKhim*. 48, 1289, 1965

[40] O.A. Timofeevicheva, P.P. Pugachevich, *Dokl. Akad. Nauk SSSR* 134, 840, 1960

[41] A.A. Karashaev, S.N. Zadumkin, A.I. Kukhno, *Russ. J. Phys. Chem*. 41, 329, 1967

[42] Kh.B. Khokonov, S.N. Zadumkin, B.B. Alchagirov, *Electrokhimiya* 10, 911, 1974

[43] S.P. Yatsenko, V.I. Kononekno, A.L. Sukhman, *High Temp. (USSR)* 10, 55, 1975

[44] Mary Eagleson *Concise encyclopedia chemistry,* 438, 1994

[45] Anthony John Downs, *Chemistry of aluminium, gallium, indium, and thallium*. Springer. ISBN 075140103X, 1993

[46] N. N. Greenwood, *Advances in inorganic chemistry and radiochemistry*, V5, 94-95, 1962

[47] S. Gowtham, A. Costales, R. Pandey, *Chem. Phys. Lett*. 431, 358-363, 2006

[48] M. Zinkevich, F. Aldinger, *J. Am. Soc.* 87 (4), 683-691, 2004

[49] W. L. Tsai, Y. Hwu, C. H. Chen, *Nuclear Instruments and Methods in Physics Research Section B* 199: 457, 2003

[50] Vigilante, G. N., Trolano, E., Mossey, C., *"Liquid Metal Embrittlement of ASTM A723 Gun Steel by Indium and Gallium"*, 1999

[51] Sublette, Cary "Section 6.2.2.1" (http:/ / nuclearweaponarchive. org/ Nwfaq/ Nfaq6. html#nfaq6. 2). *Nuclear Weapons FAQ*.. Retrieved 2008-01-24., 2001

[52] J.V. Naidich, J.N. Chuvashov, *J. of Materials Sci*ence 18, 2071-2080, 1983

[53] J.M. Chabala, *Phys. Rev*. B 46, 11 346, 1992

[54] Achieving ultralow nanoscale wear

[55] J.C. Angus, P. Koildl, S. Domotz, *Plasma Deposited Thin Films,* 1986

[56] J. Ishikawa, Y. Takeiri, K. Ogawai, *J. Appl. Phys*. 55, 188, 1987

[57] Y. Lifshitz, S.R. Kasi, J.W. Rabalais, *Phys. Rew. Lett*. 68, 620, 1989

[58] S.D. Berger, D.R. McKenzie, P.J. Martin, *Philos. Mag. Lett.* 57, 285, 1988

[59] P.J. Fallon, V.S. Veerasamy, C.A. Davis, *Phys. Rew*. B48, 4777, 1993

[60] D.L. Pappas, K.L. Saenger, J. Bruley, *J. Appl. Phys*. 71, 5675, 1992

[61] F. Xiong, Y.Y. Chang, R.P.H. Chang, *Phys. Rew*. B48, 8016, 1993

[62] H. Ehrhardt, R. Kleber, A. Kruger, *Diamond Relat. Mater*. 1, 316, 1992

[63] W. Moller, *Appl. Phys*. A 56, 527, 1993

[64] M.Weiler, S. Sattel, T. Giessen, *Phys. Rew*. B Vol.53, 3, 1594-1608, 1996

[65] K. Tachibana, M. Nishida, H. Haminas, *J. Phys*. D17, 1727, 1984

[66] Ventracor VentrAssist LVAS

[67] R. Barker, W.H.N. Hamill, R.R. Williams, *J. Phys. Chem*. 63, 825, 1959

[68] C. Pira, A. Frigo, G. Keppel, G. Lanza, S. Marigo, A. Minarello, H. Padamsee, N. Patron, V. Palmieri *New Magnetron Configurations with Enhanced Ionization Discharge for Sputtering Nb onto Cu*

[69] M. Peiniger, H. Piel, *Nuclear Science* 32 (5): 3610, 1985

[70] Salles Moura, Hernane R., *"Melting And Purification Of Niobium". AIP Conference Proceedings (American Institute of Physics) (Single Crystal - Large Grain Niobium Technology))*: 165–178, 2004

[71] Gupta, C. K.; Suri, A. K., *Extractive Metallurgy of Niobium*. *CRC Press*., 1–16, 1994

[72] Nikulina, A. V, *Metal Science and Heat Treatment* 45 (7–8): 287–292, 2003

[73] Jahnke, L.P., Frank, R.G., Redden, T.K., *Metal Progr*. 77 (6), 1960

[74] Papp, John F. *"Niobium (Columbium) and Tantalum". USGS 2006 Minerals Yearbook,* 2008

[75] Glowacki, B. A.; Yan, X. -Y.; Fray, D.; Chen, G.; Majoros, M.; Shi, Y, *Physica C: Superconductivity* 372–376 (3): 1315–1320, 2002

[76] Lilje, L.; Kakob, E.; Kostina, D.; Matheisena, A.; Möllera, W. -D.; Procha, D.; Reschkea, D.; Saitob, K. Schmüserc, P.; Simrocka, S.; Suzukid T.; Twarowskia, K., *Nuclear Instruments and Methods in Physics Research Section A: Accelerators, Spectrometers, Detectors and Associated Equipment* 524 (1-3), 2004

[77] A. Horling, L. Hultman, M. Oden, J. Sjolen, L. Karlson, *Surf. Coat. Technol*. 191, 384, 2005

[78] G. Brauer, R. Esselborn, *Z. Anorg. Allg. Chem*. 309, 151, 1961

[79] G. Capuccio, U. Gambardella, A. Morone, S. Orlando, G.P. Parisi, *Appl. Surf. Sci*. 110, 399, 1997

[80] K. Inumaru, H. Okamoto, S. Yamanaka, *J. of Crystal Growth* 237, 2050, 2002

[81] A. Aubert, J. Spritz, *Thin Solid Films* 96, 191, 1982

[82] A. Shoji, S. Kiryu, S. Kohjiro, *App. Phys. Lett.* 60, 1624, 1992

[83] T. Takahashi, H. Itoh, T. Yamagushi, *J. of Crystal Growth* 46, 69, 1979

[84] X. Liu, J.R. Babcock, M.A. Lane, J.A. Belot, A.W. Ott, M.V. Metz, C.R. Kannewurf, R.P.H. Chang, T.J. Marks, *Chem. Vap. Deposition* 7, 25, 2001

[85] M. Fenker, M. Balzel, H.A. Jehn, H. Kappl, J.-J. Lee, *Surf. And Coat. Tech*., 150, 101, 2002

[86] V. Buscaglia, F. Caracciolo, M. Ferretti, M. Mingussi, R. Musenich*, J. of Alloys and Compounds*, 266, 201, 1998

[87] H. Padamsee, A. Joshi, *J. Appl. Phys*. 50, 1112, 1979

[88] A. Darlinski, J. Halbritter, *Surf. Interface Anal*. 10, 1987

[89] K. Mbaye, M. Pham Tu, N.T. Viet, L. Wartski, J.C. Villegier*, Rew. Phys. Appl*. 20, 457, 1985

[90] J. M. Heintz, J. C. Bernier*, J. of Material Sci.* 21, 1569-1573, 1986

[91] F. Zhang, S.-W. Chan, J. E. Spanier, E. Apak, Q. Jin, R. D. Robinson, and I. P. Herman, Appl. Phys. Lett. 80, 127, 2002

[92] R.D. Green, *Carbon Dioxide Reduction on Gadolinia-doped Ceria Cathodes, Submitted in partial fulfillment of the requirements for the degree of Doctor of Philosophy. Dissertation Adviser: Dr. Chung-Chiun Liu. Department of Chemical Engineering CASE WESTERN RESERVE UNIVERSITY*, 2009

[93] Y. S. Touloukian, R. K. Kibby, R. E. Taylor, and T. Y. R. Lee, *Thermophysical Propertiesof Matter* 13, 1970

[94] D. Taylor, *Br. Ceram. Trans. J.* 83:32, 1984

[95] Semiempirical Estimation of Thermal Expansion Coefficients and Isobaric Heat Capacities of Fluorite-Type CompoundsH. Inaba1

[96] Brezesinski T, Antonietti M, Groenewolt M, *International Journal of Thermophysics* 21, 2000

[97] A. Trovarelli, *Materials Cat. Rev*. 38 439–520, 1996

[98] Properties of Common Abrasives (Boston Museum of Fine Arts)

[99] A. Tschope, W. Liu, M. Flytzani-Stephanopolous, and J. Y. Ying, J. *Catal.* 157, 42, 1995

[100] S. Park, J. M. Vohs, and R. J. Gorte, *Solid State Ionics* 12, 391, 1984

[101] H. Jahanfar, *Master Thesis Sputtering in DC, AC, RF and DC pulsed regime of a protective and transparent coating for numismatic applications*, LNL INFN, 2010